

Contents lists available at [ScienceDirect](https://www.sciencedirect.com)

Journal of Building Engineering

journal homepage: www.elsevier.com/locate/job

Analysis of structural integrity through the combination of non-destructive testing techniques in heritage inspections: The study case of San Segundo's hermitage (Ávila, Spain)

Mercedes Solla ^a, Miguel Ángel Maté-González ^b, Cristina Sáez Blázquez ^{b, *},
Susana Lagüela-López ^b, Ignacio Martín Nieto ^b

^a CINTECX, GeoTECH Research Group, Universidade de Vigo, 36310, Vigo, Spain

^b Cartographic and Land Engineering, University of Salamanca, Higher Polytechnic School of Avila, Hornos Caleros 50, 05003, Avila, Spain

ARTICLE INFO

Keywords:

Cultural heritage
Structural integrity analysis
Geophysical and optical techniques
Pathology
Methodological integration

ABSTRACT

The establishment of proper conservation and preservation actions has become one of the major concerns for historic cities. Given that possible damage affecting these buildings can be fast-acting and irreversible, the evaluation of the damage origin must be faced from the application of different prospecting possibilities adapted to the specific conditions of the approach. In this regard, the application of non-destructive testing techniques has become one of the most common practices for the characterization of pathologies in cultural heritage. The present research focuses on the analysis of the structural integrity of the Hermitage of San Segundo (center of Spain) through the application of these prospective methodologies that do not pose any damage to the asset. More specifically, the work combines geophysical and optical techniques (ground-penetrating radar, terrestrial laser scanner and drone with RGB camera, and infrared thermography) to provide a complete characterization of the analyzed building. Results show that the combination of the three non-destructive techniques allows detecting defects, defining their possible causes and providing a solid basis for future decision-making regarding maintenance and restoration actions. Methodological integration has shown that certain pathologies can only be detectable with specific techniques while others have been corroborated through the results obtained with the three testing methodologies.

Abbreviations

NDT	Non-Destructive Testing
LiDAR	Light Detection and Ranging
IRT	Infrared Thermography
GPR	Ground-Penetrating Radar
TLS	Terrestrial Laser Scanner
GSD	Ground Sampling Distance
GNSS	Global Navigation Satellite System

* Corresponding author

E-mail address: u107596@usal.es (C.S. Blázquez).

<https://doi.org/10.1016/j.job.2024.109295>

Received 14 November 2023; Received in revised form 4 March 2024; Accepted 9 April 2024

Available online 12 April 2024

2352-7102/© 2024 The Author(s). Published by Elsevier Ltd. This is an open access article under the CC BY-NC license (<http://creativecommons.org/licenses/by-nc/4.0/>).

RMSE	Root Mean Square Error
HBIM	Heritage Building Information Modelling
DT	Digital Twin

1. Introduction

Cultural heritage represents a testimony of cultural values that need to be preserved for future generations in order to understand the past architectural and archeological traditions. Cultural heritage also means a significant economic asset in regions that were historically important in the past, but have been relegated to the background in the more recent socio-economic context [1]. As shown in numerous previous experiences, the existence of a robust and well-preserved cultural heritage, accompanied by a series of strategies to promote and boost it, is proving to be an increasingly important driver of tourist attraction and cultural entrepreneurship [2].

However, the race for heritage conservation and enhancement, coupled with the implementation of these advanced cultural development strategies, is not without difficulties. The continuous testing required by most of these structures, together with the difficulty in finding economic support for the restoration and enhancement of these environments, has meant that many of the initiated projects have been shelved at very early stages of their development. The technical difficulties that often arise in the monitoring and restoration of these buildings and environments also constitute an important part of the obstacles for the promoters of the considered cultural impulse [3,4]. This paper presents a case of application of Non-Destructive Testing (NDT) methodologies that aim to contribute to the enhancement in the integration of these techniques in the combined testing of key elements in historic and cultural buildings in situations of suboptimal conservation [5]. The results obtained show that it is possible to extract relevant information about the condition of specific parts of this type of buildings by means of a global analysis of the information collected in the different tests, which adds value to the analyses that could be performed on the results of the each single test. In addition, the combination of techniques allows adapting the testing strategy according to the partial results obtained by the sensors in order to concentrate efforts in areas where one of them detects something of interest. This way of proceeding would not be possible in the case of performing tests in isolation, even if the results were then pooled for a global analysis of the monitoring.

1.1. Relevant aspects in structural conservation

Traditionally, maintenance, repair, rehabilitation and restoration are the key factors that, when coordinated represent the perfect balance in the intervention of heritage buildings. The present work seeks to show that a strategy of advanced monitoring at some points of the structural condition of the heritage can mean a great advantage in terms of the costs of repairing damages as well as an increase in the structural safety of the building itself.

The most relevant aspects to be analyzed during the punctual monitoring of historical structures can be summarized as follows.

- **Moisture.** It is a proven fact that humidity initiates degradation processes of mortar, which is often the binding element of the bricks and stones that make up the overall structure of the historic building. The carbonation processes (such as laminations, corrosions) involved with high humidity levels are known to severely affect the mechanical properties of these building elements. In addition, capillarity or the appearance of different biological colonization processes such as microorganisms (mold, fungi, bacteria, algae, etc.), mosses and liver species, or rotting can be derived [6,7].
- **Mechanical degradation of materials with structural function.** Identifying the deterioration mechanisms of the structural elements of an ancient building, taking into account the particularities due to the composition of the rocks/masonry elements used and the treatment specific to the region and the period, is fundamental to establish strategies for the conservation and remediation of existing and future defects. In this sense, the appearance of cavities, areas of less compaction or processes of erosion, washing and losses of materials is common in ancient buildings [8].
- **Appearance of defects due to overloads.** Deterioration due to anomalous load distributions, caused by changes in the geometry of structural elements, is an effect that needs to be detected as early as possible in order to develop immediate control strategies. The rate of deterioration is often very high, even endangering the structural integrity of parts of the monitored structure. These phenomena can give rise to possible cracks, fractures or displacements of the structural components [9].
- **Deformations.** Deformations in historic buildings can occur for many reasons, from the effect of local seismic phenomena [10] to the consequence of other structural defects such as anomalous load distribution, destruction of construction elements, etc. In any case, their early detection helps to mitigate the effect on the building more easily to avoid deformations on walls and columns (buckling or collapses), beams and floors (excessive lateral buckling or deflection), arches and vaults or on inclined roof elements. Furthermore, these deformations can cause other types of pathologies such as cracks. However, cracks are not only limited to structural deformations, as they can arise due to additional factors, such as changes in temperature, high levels of humidity or water infiltration, deterioration of construction materials, ground movements, building settlements, structural loads and even foundation problems [11].
- **Degradation or defects in wooden elements.** Wooden buildings are usually affected by damages derived from the appearance of moisture or microorganisms and insect damage. Termite damage is one of the most serious problems that need to be early detected for a proper conservation of the wooden building components [12,13].

As can be deduced from the above, the described causes are strongly interconnected and require a comprehensive analysis combining different methodologies that address each of the problems that may appear. In this context, the control of the pathologies can be done by means of different techniques. Destructive and non-destructive analysis can be fundamentally distinguished. For reasons

related to the high heritage value of the elements studied, the use of non-destructive tests is particularly relevant here in order to preserve the historical character of heritage buildings. With the purpose of evaluating both the visible and non-visible condition state of a historical hermitage, the monitoring strategy shown in this work is based on complementary non-destructive techniques, namely Light Detection and Ranging (LiDAR), Infrared Thermography (IRT), and Ground-Penetrating Radar (GPR). Although the present approach is applied to a particular case study, it can be extended to other situations of conservation projects. It is worth mentioning that the use of geophysics, and specifically the GPR, is suitable for the identification of inner pathologies, and probable causes, as well as for the detection of hidden elements of special interest depending on the context of the building [14]. On the other hand, LiDAR technology uses laser pulses to generate a three-dimensional map with information about the intensity of reflections or even in colour if the device is equipped with an RGB sensor, thus providing a detailed representation of a surface. In this way, it is possible to detect structural pathologies such as collapses, cracks, erosion or deformations. Other pathologies, such as humidity, can also be located through an image of the intensity generated by the LiDAR. Finally, infrared thermography measures the thermal infrared radiation emitted by the bodies due to their temperature condition, in such a way that it makes possible to detect temperature differences on the surface of the building, which can be useful to identify problems such as heat loss, humidity or other irregularities, from the analysis of the thermal print.

1.2. Review of optical and geophysical techniques in heritage buildings

Given the importance of addressing the control of the cultural heritage state, geophysical techniques stand out as one of the preferred tools for the diagnosis of inner pathologies and the definition of repair prognosis. Moreover, integrated geophysical and optical surveys allow comparing results obtained by different methods to finally infer details about the heritage building. The superposition of these non-destructive tests ensures the exclusion of possible ambiguities and allows complementing the results for an exhaustive knowledge of the case under study; thus contributing to the documentation of both visible (optical) and non-visible (geophysical, optical) elements [15].

In this sense, geophysical techniques have been applied on numerous cases, and for multiple purposes, in the field of heritage. Among the different non-destructive methods, mechanical and electromagnetic technologies are especially important for structural imaging [16]. Within the electromagnetic surveys, the GPR is one of the most used methodologies due to its high resolution and applicability in heritage and civil engineering [17], in addition to its easy portability, due to its reduced weight and size (compared to other techniques) [18]. Given the popularity of this technique in testing slabs, floors or underground objects, numerous examples of its application can be found in the published literature. Perez-Garcia et al. [14] analyzed the GPR signal for the identification of moisture in heritage buildings. Drobiec et al. [19] studied the possibility of detecting spaced rebars in concrete specimens based on GPR time-slices (or C-Scans). Novo et al. [20] applied a 3D GPR methodology to detect and reconstruct a buried sarcophagus.

Regarding the inferring of mechanical properties, the use of computed tomography, both microwave and ultrasound tomography techniques have been widely implemented for the inspection of masonry objects and concrete. Binda et al. [21] analyzed stone piers of the Notho Cathedral using sonic and radar tomographic imaging. Zendri et al. [22] applied ultrasonic tomography for the investigation of historical columns before and after consolidation interventions. Shiotani et al. [23] studied a deteriorated pier in a concrete dam by using ultrasonic transmission tomography for evaluating the repair effect before and after grouting. As a final example, Haach and Ramirez [24] evaluated the influence of different discontinuities and arrangements of transducers from the results of the tomograms of concrete prisms.

As a common practice, when different mechanical and electromagnetic parameters from constructive materials must be inferred, the combination of the mentioned and other prospecting possibilities is required. Integrated aerial imagery and photography and several geophysical techniques, such as GPR, Electrical Resistivity Tomography (ERT) and magnetic resonance imaging, were used in the archeological site of the Roman town of Carnuntum [25], the largest archeological landscape in Austria. The investigation resulted in accurate high-resolution outlines of both visible and buried structures on the overall site. In the case of the village of Takamatua, New Zealand, a combination of total-field magnetic, horizontal loop electromagnetic, GPR, and ERT techniques allowed to detect linear anomalous responses that verified the initial hypothesis about the presence of a blockhouse [26]. A combination of GPR and seismic tomography is presented in Pérez-Gracia et al. [27] for evaluating the supporting structures (columns, walls, and buttresses) of the Mallorca Cathedral in Spain.

In addition to geophysical techniques, the use of optical methodologies has also become a common standard when it comes to monitoring and diagnosing the pathologies mentioned in cultural and architectural heritage. In this sense, multispectral radiometric analysis has been implemented for recognizing pathologies in historical buildings by the use of remote sensing techniques [28,29]. Beyond this, IRT has been widely applied for the evaluation of heritage sites, as studied in Ref. [30], from the detection of pathologies to the discovery of buried goods [31] and the large-scale determination of heritage sites if the inspection is performed from an aerial platform [32]. Regarding the first application listed, the pathologies that can be analyzed from a thermographic inspection are those that can have an impact of the thermal footprint. In this line, IRT can be used for the detection of superficial pathologies such as cracking [33], delamination and detachment [34]; but also of sub-superficial problems that have an affection in the surface like moisture and water infiltration [35] and corrosion [36]. The level of penetration of the thermographic survey depends on the level of thermal excitation of the sample and on the severity of the pathology. In addition to pathology detection, IRT can be used to characterize materials with their thermophysical parameters [37], in such a way that the conservation state of surfaces with no explicit defects can also be determined.

In addition to its standalone capacity, IRT has been successfully implemented in different sectors and fields to enrich inspections performed with geophysical and spatial data. With respect to the GPR and IRT combination [15], has analyzed existing studies with different applications including cultural heritage; in the heritage sites study, the combination of techniques has as main contribution

the detection of moisture and the determination of the water path [38], although some case studies have been developed in which IRT and GPR techniques have been conjointly applied for the detection of hidden structures [39]. Regarding the combination of IRT with spatial data obtained from other approaches such as digital photogrammetry or Terrestrial Laser Scanner (TLS), it allows the study of the pathologies detected from their thermal print in 3D, as well as the better detection of pathologies thanks to the analysis of the temperature distribution along the three dimensions. This is because the active survey technique TLS allows the acquisition of high density 3D point clouds that can be applied in the reconstruction of geometrically faithful representation of surfaces [40]. Regarding photogrammetry, it provides an estimation of the 3D coordinates of common points in different photographs to finally create three-dimensional realistic models [41]. Different techniques have been developed for the thermographic 3D modelling of cultural heritage [42]: shows that the combination of range and image-based data and thermal information is capable of providing a complete documentation of heritage and archeological sites; while in Ref. [43], the combination of IRT with TLS was evaluated as a projection of thermograms in the point cloud for the study of a certain historic building in 3D.

More information and possibilities of combination for optical and geophysical techniques applied to the assessment of heritage buildings can be found in Refs. [44–53]. Combining these techniques often involves interdisciplinary research, and papers that specifically address the integration of multiple methodologies may be found in journals focusing on heritage conservation, structural engineering, and geophysics. Since the field is dynamic, new works are emerging at an ever-increasing rate, presenting new variations and integration of technologies, as well as innovations in the different processes involved in the entire data collection and post-processing.

Considering the possibilities of the existing technologies, and their combination, this research focuses on the application of TLS, IRT and GPR for the identification of possible pathologies and findings of interest in the cultural asset Hermitage of San Segundo. It has a Romanesque style with historical value, which is of great interest because it consists of different construction materials (stone, cement, and timber), as well as different pathologies (structural deformations, moisture and detachments, etc.). As demonstrated in the review above, the individual use of the selected techniques has been recognized as efficient tools in the evaluation of this type of heritage buildings, with numerous successful works in the published literature. However, the combination of NDTs proposed herein is still not sufficiently addressed. The combination of IRT and GPR applied to the moisture detection and its distribution has been widely used in stone and cement elements [54,55] but, to date, no studies have been found for this combination in timber elements. As shown in the following sections, the application of the geophysical and optical techniques selected in this work provides complementary results that contribute to achieving thorough knowledge about the case under study. The work is structured as follows; a first description of the case study is provided in section 2. Section 3 presents a brief introduction to the prospective techniques considered. Section 4 describes the results of the application of each of the mentioned techniques. Section 5 covers the integration and complementarity of the proposed methodologies including the conclusions reached with the combined study.

2. Case study

2.1. History

The Hermitage of San Segundo is located outside the walls of the region of Ávila, being the westernmost of the city temples, placed at a lower altitude on the banks of the Adaja River. The church was initially dedicated to San Sebastián and Santa Lucía, but in 1519, a stone chest was found with the inscription of "Santus Secundus" also containing another wooden trunk with bones, ashes, remains of clothing, a gold ring, and a chalice. These findings led to belief that the remains could belong to the San Segundo Apostle, the first bishop of Ávila and the founder of the city.

The remains of San Segundo were transferred to the cathedral of Ávila at the end of the 16th century. Since then, the hermitage was renamed San Segundo, and the cult of San Sebastián moved to a small shrine at outskirts of the city. With the new dedication to San Segundo, the region began to have a sentimental link with the church which was declared National Monument in 1923 [56].

2.2. Construction materials and structural approach

The construction of the temple is estimated between 1130 and 1160, as it is contemporary and traditionally associated with the church of San Andrés (center of the Ávila city).

San Segundo hermitage is constituted by a three-nave plan and a deviated tripartite apse, sometimes related to the inclination of Christ's head on the cross, although this explanation does not seem plausible, being the most likely causes the irregularity of the ground, a mistake of the builders or even the existence of some structure of a previous cult. The hermitage is of Romanesque style and only preserves the triabsidal apse, the south portal, and the load-bearing walls.

The temple stands on a plinth of granite ashlars, on which rows of ocher granite of caleña stone (sandstone) rise. The head, topped with nacelle corbels, has no openings and some later buildings were added to its northern part, while the interior is covered with a barrel vault and oven. The naves were dismantled in 1519 and rebuilt by the stonemasons Lázaro de la Peña and Pedro de Huelmes, while the wooden framework was made in 1521 by the carpenter Rodrigo de Matienzo [57].

The west door dates from the 17th century, being in Baroque style. It is constituted by a large basket-handle arch and an oculus above it. For its part, the south door is Romanesque in style, flared and semicircular, and decorated with archivolt rosettes on smooth jambs and columns, and even a bird with outstretched wings that decorate the capitals. It is estimated that two sculpture workshops were involved in the construction of the hermitage, one working on the header, and one on the cover, around the second third of the 12th century.

With the passing of the centuries, the church of San Segundo has undergone great transformations, such as the construction of a small sacristy, or the large arches that separate the naves and support the framework and wooden roofs. It is also curious the construction attached to its north wall, today in ruins, which belongs to the first settlement of the Calzada Carmelites in Ávila, back in 1600

[58]. The latest restoration works on the hermitage have focused on the roofs, allowing the temple to continue being visited while preserving the original vestiges of the past.

3. Materials and methods

3.1. Ground-penetrating radar (GPR)

Different GPR surveys were conducted to investigate hidden elements and structural defects on the hermitage of San Segundo. A ground-coupled system manufactured by Malå Geoscience was used, consisting of a ProEx control unit and bistatic antennas. As described in Table 1, the central frequencies of the antennas and the setup used for data acquisition were varied depending on the purpose.

Three-dimensional (3D) GPR methodologies were carried out for the cases 3 (2.3 GHz) and 4 (1.2 GHz) in Table 1, with a total of 11 parallel profile lines at regular intervals of 12 cm spacing, and 33 parallel profile lines at regular intervals of 10 cm spacing, respectively.

The GPR raw data collected in this work are openly available in Zenodo [59].

The GPR signals received were processed with the ReflexW software by applying the processing sequence described in Table 2. The processed data were then exported to the 3D data interpretation module of the same processing software for the 3D cube generation. This 3D cube allows for the extraction of vertical (XZ and YZ) and horizontal (XY or time-slice) images to enhance visualization and the spatial correlation of the reflectors.

3.2. Terrestrial laser scanning (TLS)

A Terrestrial Laser Scanner was used in this research to obtain a detailed model of the interior of the hermitage and its main façade (see Fig. 1). More specifically, the lightweight terrestrial laser scanner Faro Focus 3D was the one employed in the work (Fig. 2). This device measures distances using the principle of phase shift (transmits continuous 905 nm laser light) within a range of 0.6–120 m, with a measurement rate of 976,000 points per second, an angular resolution of 0.009°, and a beam divergence of 0.19 mrad. Concerning its accuracy, this laser allows for capturing scenes with ± 2 mm of precision under normal lighting conditions.

It must be also mentioned that, in order to precisely align the different scans made both outside and inside the church, six registration spheres of 145 mm diameter were used. The most representative raw TLS data used in this research are openly available in Zenodo [60].

3.3. Drone + RGB camera

A DJI Mavic 2 Pro was used to capture the images from two flights applying the protocols below. In the first place, a drone flight was carried out following a parallel data collection protocol of all the façades of the church. Images with overlaps of 70 % (front overlap, relative to the direction of flight) and 40 % (side overlap) were captured. Finally, 300 images collected at a flight height of 5–8 m

Table 1
Different targets assumed for the GPR surveys and setup used for data acquisition.





	1) Moisture detection in the side wall of the altar	2) Characterization of the stonework materials in the main façade		3) Inner defects (e.g. cracks or voids) in wooden beams		4) Detection of hidden tombs
						
Antennas	2.3 GHz	2.3 GHz	1.2 GHz	2.3 GHz	1.2 GHz	1.2 GHz
Trace-interval	4.5 mm	4.5 mm	10 mm	4.5 mm	10 mm	10 mm
Time window	11 ns	11 ns	25 ns	11 ns	25 ns	25 ns
Samples per trace	376	376	424	376	424	424

Table 2
Filters and parameters used for GPR data processing.

Filters	Parameters	
	2.3 GHz	1.2 GHz
Time-zero correction	−1.1 ns	−3.2 ns
Subtract-mean (dewow)	Time window: 0.4 ns	Time window: 0.8 ns
Gain function	Linear: 2.88 and Exponential: 2.88	Linear: 2 and Exponential: 2
Background removal	By default	By default
Div. compensation	Factor: 1.44	Not applied
Bandpass (Butterworth)	Lower: 1384 and Upper: 4942 MHz	Lower: 692 and Upper: 1830 MHz
Migration (Kirchhoff)	Velocity: 0.1 m/ns	Velocity: 0.1 m/ns



Fig. 1. Location and details of the hermitage of San Segundo.



Fig. 2. Detailed view of the Faro Focus 3D 120 Terrestrial Laser Scanner used in this research (left) and during the data collection in the hermitage under study (right).

and at a distance of 6–8 m from the building (when possible) were obtained, estimating a Ground Sampling Distance (GSD) value of 0.5 cm. Secondly, for the global documentation of the hermitage, photographs were taken from the drone following an oblique/convergent photographic protocol. These photographs were taken ensuring an adequate overlap between the images (around 80–90 %), with a separation between them of 10 to 15° and maintaining a constant distance from the building (when possible). To perform this task, a series of photographs were taken in a single flight following a circular sequence (360°) centering the point of view of each image towards the center of the building, flying in a circular fashion at three heights above the ground (4 m the camera being perpendic-

ular to the church, 10 m with a camera tilt of 70° and 25 m with a camera tilt of 50°). Finally, a total of 254 images were obtained, estimating a mean GSD value of 1 cm.

In addition to the above, a total station (Leica TCRM1203+R1000) was used to obtain information from natural points evenly distributed on the east and south façades, with a precision of ± 0.2 cm. For this work, only one station point with known coordinates and two other points (also with known coordinates) were used to orient the equipment. The absolute coordinates of the three points were measured with a Global Navigation Satellite System (GNSS) (Topcon GR-5), with an accuracy of ± 1 cm. The details of the façades from which the coordinates were obtained were easily identifiable in each of the photographs, which allowed resolving the external orientation and georeferencing of the subsequent analyses.

Once the two flights were performed with the drone, all the images were processed with a photogrammetric reconstruction software. This reconstruction was performed with the open-source photogrammetric software GRAPHOS [61].

3.4. Infrared thermography (IRT)

The thermographic inspection was performed with the aim at detecting in the church the thermal pathologies that are most commonly detected with this technique in cultural heritage; that is, moisture areas, delamination, air leaks, corrosion and efflorescence. As this is the objective, the measurement of absolute temperature is not required, in such a way that a qualitative analysis is performed. For this reason, the calibration of emissivity value is set to 1, and reflected temperature, ambient temperature and humidity were not taken into account. Under these circumstances, it should be highlighted that temperatures measured are apparent temperatures and not absolute values.

Regarding equipment, the thermographic camera NEC TH9260 is used. This is a non-refrigerated thermographic camera, handheld by the operator. Its technical characteristics are shown in Table 3.

With respect to the external conditions, the inspection was performed on a day with adequate thermographic conditions; that is, no rain in the previous 24 h in order to avoid measuring remaining wetness and confuse it with real moisture pathologies, and no wind with the aim at avoiding the disturbance this event provokes in the temperature print. Last, the thermographic inspection was planned in such a way that the external walls were inspected with no direct Sun radiation and the internal inspection was performed at midday hours in order to maximize the temperature difference between the exterior and the interior of the church. In this way, the thermal print of the pathologies is highlighted while applying the passive thermography approach.

The IRT data acquired during this work are publicly available in Zenodo [62].

4. Results

4.1. Integration of TLS and photogrammetry

In order to capture the entire interior of the church in detail and part of its exterior façades, a total of 21 scans were made (Fig. 3). The alignment of these scanning stations was carried out using the goal-based registration method. This method allows different point

Table 3
Technical specifications of the thermographic camera NEC TH9260.

Model	NECTH9260
Sensor type	Uncooled focal plane array (μ bolometer)
Thermal image/pixels	640 (H) x 480 (V)
Resolution ($^{\circ}$ C)	0.1
Accuracy	± 2 $^{\circ}$ C or ± 2 % of reading, whichever is greater
Spectral range (μ m)	8 to 14

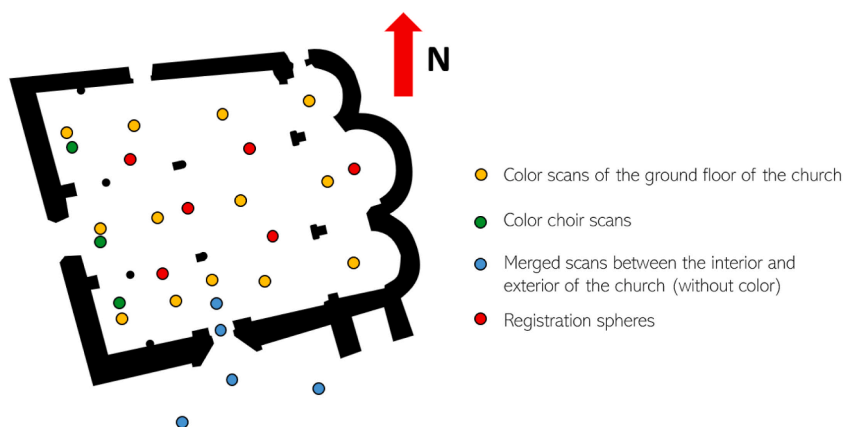


Fig. 3. Location of the scans and registration spheres used in the research.

clouds to be aligned by using geometric features from artificial targets such as planar targets or registration spheres. For the present case study, a goal-based registration approach capable of using the centroid of each registration sphere as a control point for the alignment between point clouds was used. In this context, RANSAC Shape Detector algorithm was applied for extracting the centroid of each of the spheres. In order to compensate possible errors of alignment, spheres were placed evenly distributed throughout the space. In this way, at least four spheres were visible from each scanning station. In addition, the scan placed in the center of the church was able to simultaneously collect the already mentioned section six spheres, being this scan used as the basis to align the set of point clouds. As a result of the above, all point clouds were aligned with an accuracy of ± 3 mm, to finally obtain a point cloud of 748,458,257 points.

On the other hand, thanks to the software GRAPHOS, the dense point cloud was generated (Fig. 4) and, as shown in Fig. 5, different orthophotos of the church façades were obtained (final results: GSD of 1.2 cm, Root Mean Square Error (RMSE): 0.8 cm, resulting from the residual errors in the control points (considering the use of 40 control points obtained with the total station)). The resulting point cloud has 200,054,752 points.

Subsequently, the previous clouds were aligned following the Cloud-based Registration method. This methodology uses as a base three common points of the two-point clouds and the software itself refines the fine record from the geometry using the common parts of both point clouds (RMSE = 4 mm). The point cloud used as a base was the one obtained by photogrammetric methods. This process was as described since the point cloud was expressed in absolute coordinates, resulting from the classical topography techniques applied on the façade. In order to verify that the point clouds were correctly aligned, coordinates of the points of the façades



Fig. 4. Top, TLS point cloud. Bottom, point cloud obtained by photogrammetric methods.

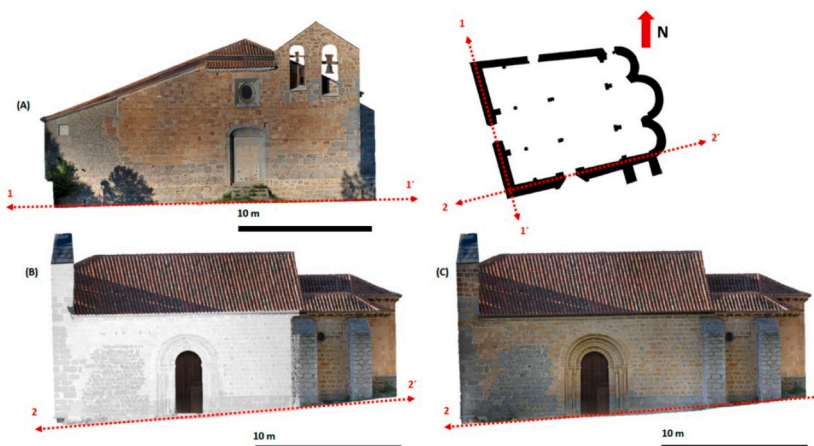


Fig. 5. Orthophotos of the two main façades of the church. (A) South façade RGB orthophoto. (B) Intensity orthophoto of the TLS east façade. (C) East façade RGB orthophoto.

obtained by classical topography methods were compared (since these points could also be easily located in the TLS cloud). As a result of this comparison, it was possible to obtain a RMSE between the two point clouds of 4 mm, with an average error of 6 mm (Fig. 6).

From the previous integration of point clouds, it is possible to obtain data about the state of the heritage building as shown in the following subsections.

4.1.1. Laser scanning intensity data applied to damage detection

As a result of the scan, a point cloud is obtained, including the coordinates of the collected points as well as their corresponding intensities. From this information, it is possible to obtain the photographs of the scanned environment. Spectral classification techniques are also used in this sense thanks to the fact that materials have different reflections depending on the wavelength. The classification consists of forming a cluster of each class of object from common neighboring pixels. From this step, classification techniques are able to reduce the range of values of the image (digital number) to another level (classes) through an allocation statistics system. In this context, numerous classification methods can be found with different levels of complexity, including hard and soft classifiers, non-parametric and parametric techniques and supervised and unsupervised methods [63]. The whole procedure of the mentioned methodology, once the image intensity has been obtained, is presented in Fig. 7.

The algorithms used for the cluster analysis in the commercial digital processing software PCI Geomatic (version 9.1) were selected for the pixel-based unsupervised classification [64,65]. For the classification, Isodata algorithm, k-means algorithm and Fuzzy k-means algorithm have been used in this research.

It is convenient to mention that the described methodology has been applied in two areas of the church. The first one, in the wall of the south façade (Fig. 8ab – orthogonal view of the interior and exterior of the wall) and the second in the lateral area of the altar, where a high degradation of the materials can be seen (Fig. 8c – side view). Each of these zones has been independently analyzed.

Before the unsupervised classification, in the three study areas, sixteen predefined classes were chosen for analysis in the classification algorithms. Some of the classes were not represented in the results map since fewer elements were available to classify. As a result of the analyses, in all cases the resulting map showed the existence of affected areas.

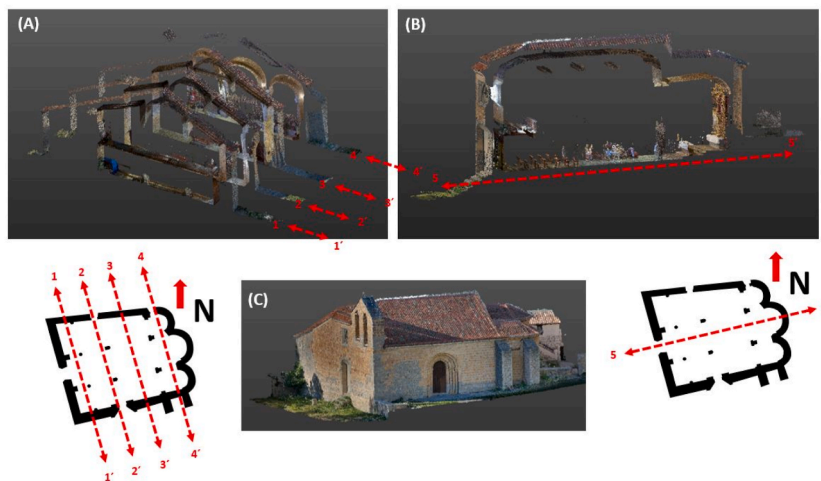


Fig. 6. Fusion of the TLS point cloud and point cloud obtained by drone photogrammetric techniques. (A) Different cross sections of the building. (B) Longitudinal profile of the building. (C) Merging of the two point clouds.



Fig. 7. Schema of the methodology presented once the image intensity is obtained.

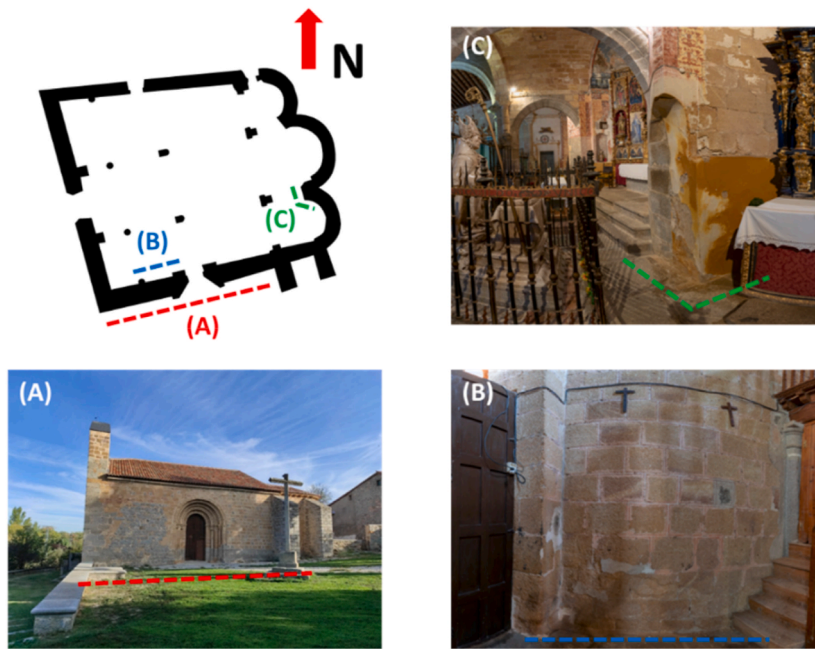


Fig. 8. (a) and (b) south façade wall, interior and exterior of the wall. (c) View of the altar.

In the first case, the external wall of the south façade was analyzed. Fig. 9 shows the classification obtained in the identified classes, which are: unaltered granite (in two levels, without deposits and without moisture evidence), altered granite (in four levels, with a high rate of erosion), lime/mortar remains and ashlar with high moisture content.

The results of the statistical analysis for each algorithm are included in Table 4. Additionally, the producer's accuracy and the user's accuracy are presented in Table 5 for each of the four classes and for each classification algorithm.

As can be observed in the above Table 4, a good relation between the number of pixels classified in a correct way and the global number of pixels is obtained, as deduced from the value of the overall accuracy for the Fuzzy k-means algorithm (was 94.45 %). It is also possible to observe that this algorithm presents the best classification results with an improvement of 0.89 in the kappa coefficient.

Analyzing Tables 5 and it is shown that the producer's accuracy for the unaltered granite class was of 93 % for the Fuzzy k-means algorithm and 85 % and 84 % for the k-means and Isodata algorithms, meaning that about 9 of 10 pixels that belong to areas of this type (unaltered granite) were included in the global unaltered class. In the rest of classes, values range from 85 to 79 % for the Fuzzy k-means algorithm to 82-71 % for the other two algorithms. In the case of the user's accuracy, in those cases with values above 85 %, 4 out of 5 pixels placed in these classes (unaltered and altered granite) represent areas with this kind of conservation problem. In the other two classes (lime and mortars remains and moisture) values indicate that a lower number of pixels represent areas with this conservation issue.

In the second case, the wall of the south façade was analyzed from the inside. Fig. 10 shows the classification obtained in the identified classes, which are: unaltered granite (in two levels, without deposits or without moisture evidence), altered granite (in four levels, with a high rate of erosion) and lime/mortar remains.

As in the previous case, the values of the statistical measures are included in Table 6, while the producer's and user's accuracy for each class and for all the algorithms considered in this work are presented in Table 7.

Results of Table 6 show that the classification system has also a great performance and that the best results are again obtained using the Fuzzy k-means algorithm.

Analyzing now the producer's and user's accuracy of Tables 7 and it was found that for all classes that aims at distinguishing the value of the producer's accuracy, the Fuzzy k-means represent the highest values with the maximum of 91 % in the unaltered granite class. Considering now the user's accuracy, the great results show again a high probability that randomly selected and classified pixels were correctly assigned in a class.

And finally, in the third case, the side wall of the altar was considered for its analysis. In Fig. 11 it is possible to observe the classification obtained from the humidity of the wall and the damage it causes.

From the statistical analysis of the following Table 8, it is seen that the value of the global precision of the Fuzzy k-means algorithm was 63.44 %, which indicates that the classification performed has a lower precision than in the previous assumptions. In this case, the best classification results were also found for this last algorithm, which presented an improvement of 0.52 with respect to a random classification.

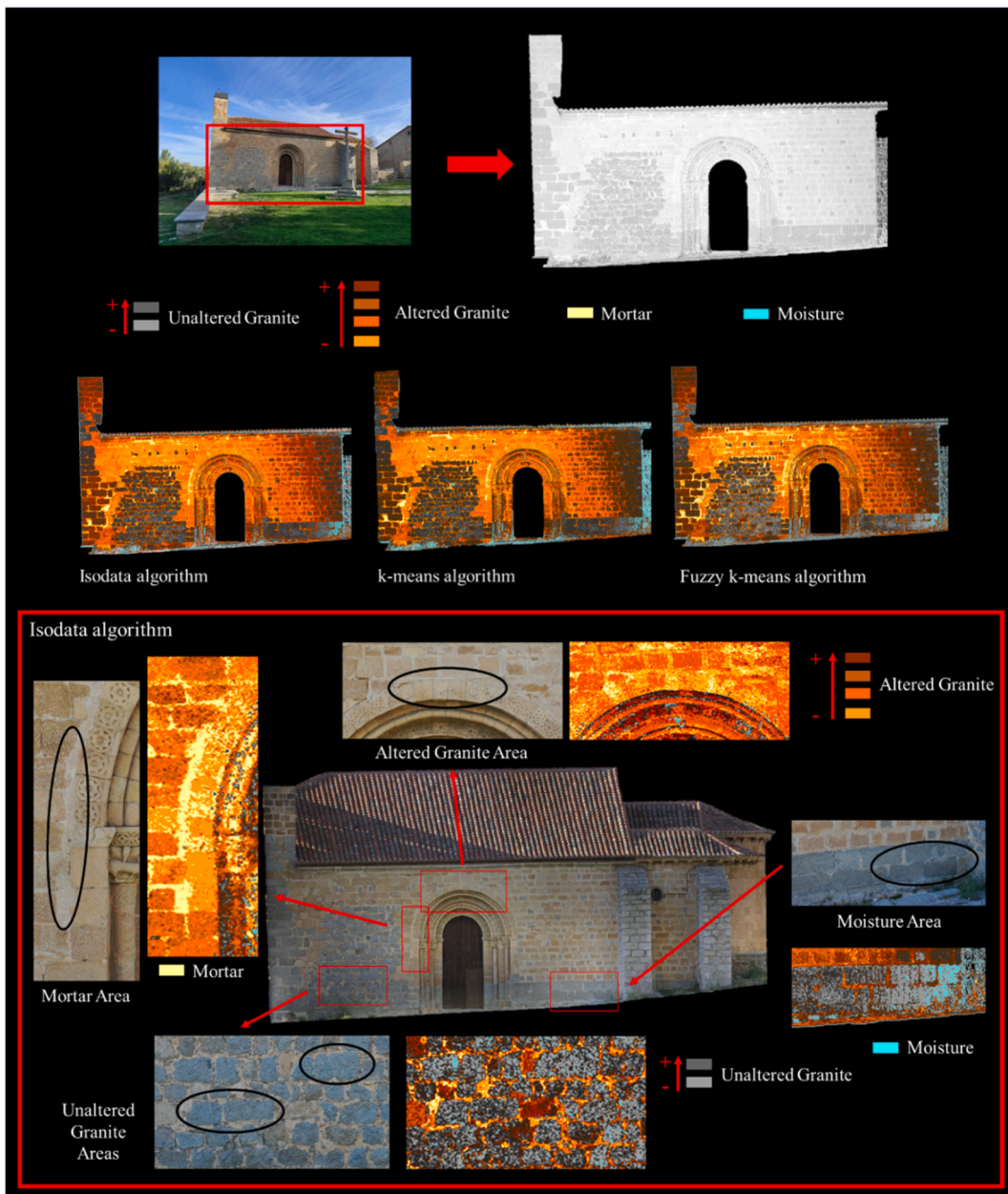


Fig. 9. Results of the unsupervised classification for each of the algorithms applied in the external wall of the south façade. \pm signals of the scale refer to the level of alteration in each granite typology.

Table 4

Accuracies obtained in the unsupervised classification for each of the algorithms implemented for the study case of the south façade external wall.

Type algorithm	Overall accuracy (%)	Kappa coefficient
Isodata	76.45	0.65
k-means	82.35	0.85
Fuzzy k-means	94.45	0.89

Table 5

Producer's accuracy and user's accuracy obtained for each of the considered clusters and for each of the algorithms included for the study case of the south façade external wall.

Type algorithm	Producer's accuracy (%)				User's accuracy (%)			
	Unaltered granite	Altered granite	Lime/mortars remains	Moisture	Unaltered granite	Altered granite	Lime/mortars remains	Moisture
Isodata	84	82	71	75	85	83	75	72
k-means	85	80	72	74	87	81	79	75
Fuzzy k-means	93	85	80	79	94	86	81	78

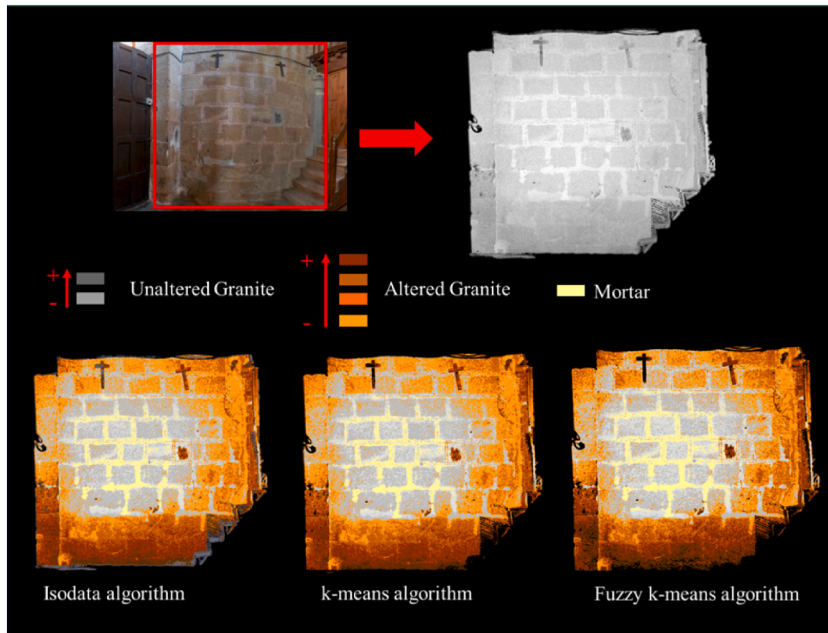


Fig. 10. Results of the unsupervised classification for each of the algorithms in the internal wall of the south façade. \pm signals of the scale refer to the level of alteration in each granite typology.

Table 6

Accuracies obtained in the unsupervised classification for each of the algorithms implemented for the study case of the south façade internal wall.

Type algorithm	Overall accuracy (%)	Kappa coefficient
Isodata	81.25	0.75
k-means	85.33	0.88
Fuzzy k-means	86.54	0.91

Table 7

Producer's accuracy and user's accuracy obtained for each of the considered clusters and for each of the algorithms included for the study case of the south façade internal wall.

Type algorithm	Producer's accuracy (%)			User's accuracy (%)		
	Unaltered granite	Altered granite	Lime/mortars remains	Unaltered granite	Altered granite	Lime/mortars remains
Isodata	82	81	75	82	82	75
k-means	84	83	76	86	81	78
Fuzzy k-means	91	84	79	92	82	78

Regarding the producer's and user's accuracy, [Table 9](#) shows that the value of the producer's accuracy for the moisture class was higher in the Fuzzy k-means algorithm. For all the algorithms considered in the user's accuracy values range 42–45 % which indicates the low probability that a pixel selected randomly and classified in the class was correctly assigned.

4.1.2. Point clouds for structural analysis

From the point cloud, it is also possible to perform visual analysis to locate damage in the building structure. For this type of analysis, it is frequent to carry out longitudinal and transversal profiles, which reveal the skeleton of the building. In these profiles, a simple

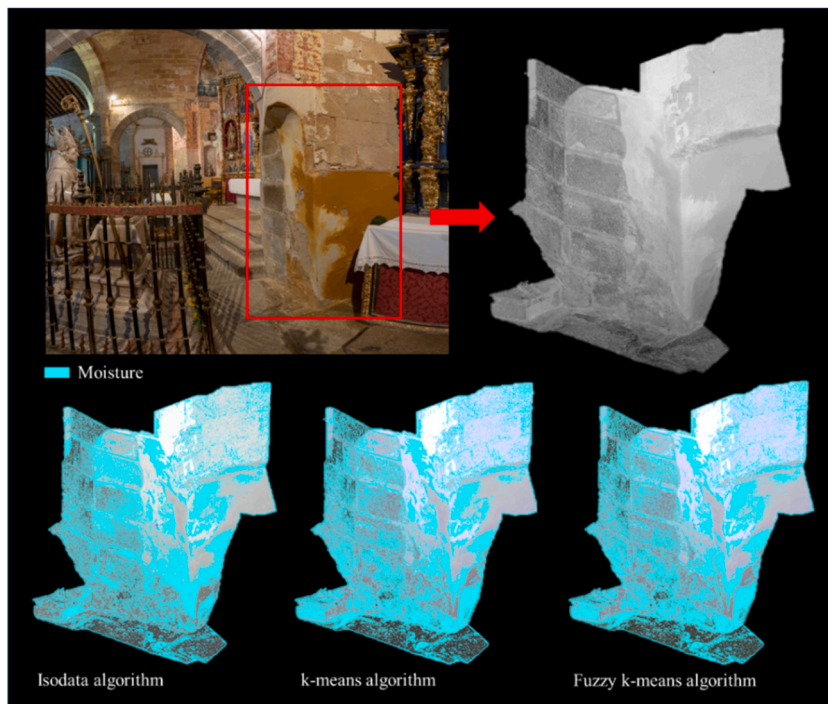


Fig. 11. Results of the unsupervised classification for each of the algorithms in the side wall of the altar.

Table 8

Accuracies obtained in the unsupervised classification for each of the algorithms implemented for the study case of the side wall of the altar.

Type algorithm	Overall accuracy (%)	Kappa coefficient
Isodata	45.35	0.45
k-means	58.23	0.48
Fuzzy k-means	63.44	0.52

Table 9

Producer's accuracy and user's accuracy obtained for each of the considered clusters and for each of the algorithms included for the study case of the side wall of the altar.

Type algorithm	Producer's accuracy (%)		User's accuracy (%)	
	Moisture		Moisture	
Isodata	45		42	
k-means	47		43	
Fuzzy k-means	65		45	

and quick inspection can be made to locate critical or damaged areas in the assets. In the case of the Church of San Segundo, the north-south cross section shows a great deformation in one of its arches (Fig. 12). This deformation is the result of a north-south lateral thrust of the main nave on the south façade. With the objective of minimizing this damage, two buttresses were built on the south façade. Given that these buttresses are made with a type of stone different from that used in the original construction, it may be concluded that they were added at a later time, although it is not exactly known when.

Furthermore, thanks to the point cloud it is possible to locate other types of deformations or collapses in the walls, comparing the morphological discrepancies between the scanned model (which would be a reliable reflection of the current state of the heritage asset) and a theoretical model (that is, a wall without deformations). Through this comparison, maps can be extracted for analyzing flatness, slopes, structural deformations, collapses, etc. This kind of analysis applied to the south façade of the building here considered can be seen in Fig. 13, in which chromatic patterns applied to the point clouds have allowed the detection of the façade deformations. For this, the theoretical plane that best fits the point cloud of the wall has been developed for subsequently define the difference in distance between the plane and the point cloud (Fig. 13) through the use of the “Compute cloud/mesh distance” tool, in CloudCompare software [66]. This is the plane that best fits the position of an even mesh of points on the façade.



Fig. 12. North-south cross section of the church.

On the other hand, as already mentioned, deformations can cause other types of pathologies such as cracks. Fig. 14 shows how through the cloud of points it is possible to analyze the cracks, being able to evaluate their shape and size, which also will contribute to define their origin.

All of the above analyses are generally complemented by regular scans over time, in order to track conditions and detect significant changes. This type of technology serves as an early warning system to notify conservation managers of unusual or dangerous deformations.

It is also important to highlight that the point cloud is the essential foundation for the development of other analysis techniques. These include the evaluation of loading conditions, as well as the use of models based on FEM (Finite Element Method) and technologies such as CAD/CAE/CAM, HBIM (Heritage Building Information Modelling) and DT (Digital Twin). The point cloud provides the initial and detailed information needed to feed and support these advanced approaches, ultimately enabling a more complete and accurate understanding of architectural structures and their pathologies.

4.2. GPR surveys

Fig. 15 presents the results obtained from the GPR survey aimed to detect moisture in the side wall of the altar (case 1 in Table 1). First, Fig. 15-a shows the 2.3 GHz data obtained at the lateral wall of the right nave of the altar. In this wall it is possible to observe detachments of the render painting, as well as stone disintegration. Observing the interpretation of the GPR data produced (profile line P1), moisture was identified in the form of parallel continuous reflections, like a reverberation, with higher amplitude values (from 3 ns to the end of the radargram in the time axis). It is more certainly indicating the presence of moisture accumulated in the interior of the stonework, giving higher dielectric contrast between media (stone and water). On the other hand, Fig. 15-b displays the 2.3 GHz data obtained at the front wall separating the main and right naves of the altar. As seen in the picture, there are two different types of stone in this sector (red dashed line). Observing the signal behavior through the stone at the left, or main nave of the altar, it is possible to detect the interface between consecutive blocks (orange dashed line). However, the situation is much different in the stone at the right, or the right nave which was built later, showing critical disintegration. For this case, the GPR signal shows severe attenuation and losses of information due to the presence of salts from the demineralization of the stone. In this sector, water would have dissolved the internal salts of the stone, dragging and depositing them on the surface (spots typically known as efflorescence). The stone has therefore lost internal consistency because it has been demineralized, leaving an external protective mineral layer. When this mineral layer disappears (e.g., through cleaning interventions), the stone is completely exposed to disintegration.

Figs. 16 and 17 present the results produced for the characterization of the stonework materials in both the external and internal wall of the main façade, respectively) (case 2 in Table 1). The radargrams produced for the external wall allowed for the identification of different ashlar in depth (highlighted with orange lines). These reflections show complex reflections patterns most certainly due to the irregular shape of the stones. Moreover, observing the radargrams in Fig. 16, it is possible to appreciate a signal attenuation at the beginning of the image (highlighted into an orange box) coinciding with a different type of stone, which most probably contributes to accumulating higher moisture. Regarding Fig. 17, the radargrams produced in the internal wall of the façade show severe attenuation, especially in the lowest profiles (e.g. profile P4), most probable due to higher moisture content, showing a similar signal behavior described for Fig. 15-a. Moreover, in both internal and external wall, a different stone was identified (highlighted into a blue ellipse) showing a prominent and complex reflection pattern. All these results demonstrate the capabilities of the GPR signal to identify different materials in the stonework (dry/wet stone, irregular/regular shapes, etc.), as well as to estimate thicknesses (if the velocity of propagation of the signal is calibrated).

Fig. 18 shows the results obtained from the GPR survey carried out to detect inner defects in wooden beams (case 3 in Table 2). The 2.3 GHz data revealed the presence of cracks and voids, showing their typical reflection pattern in the form of small hyperbolas. However, the poorer resolution of the 1.2 GHz antenna was not enough to detect such features. Observing the interpretation of the radargrams produced in Fig. 18, the defects were detected to occur at the first 1 ns. Considering a velocity of propagation of the GPR signal into wood of about 13.5–17.4 cm/ns [67], it means a depth of about 6.7–8.7 cm.

Fig. 19 presents the 3D time-slice (XY image) produced at 0.3 ns (approx. 2.0–2.5 cm deep) in the wooden floor. Observing the interpretation of the time-slice, it was possible to map a region of irregular reflection patterns (highlighted into a dashed red line),

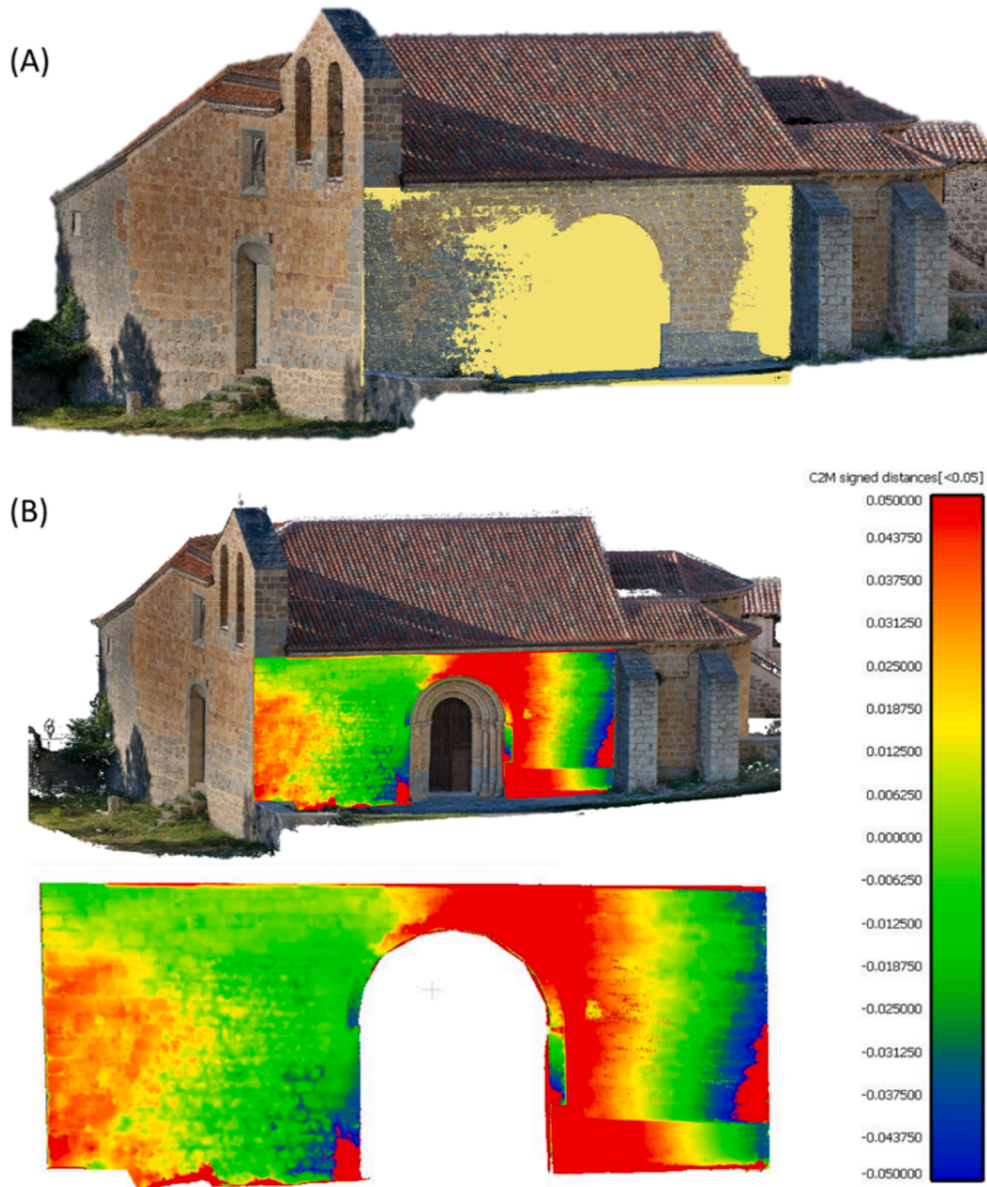


Fig. 13. (a) Plan that best fits the wall of the south façade. (b) Image of façade flatness analysis.

instead of the linear beams identified in the rest of the image. As the media is homogeneous wood, this effect is most probably produced by a different wood condition, with different media permittivity due to moisture. It should be mentioned here that the length of the profile lines, in the X direction, was variable, and the grey areas means non data.

Fig. 20 shows the results produced for the 3D GPR survey carried out at the area of the tombs (case 4 in Table 1). The resulting time-slices and YZ images generated from the 3D cube permitted the visualization of two stronger reflectors interpreted as hidden tombs.

4.3. IRT inspection

From the thermographic inspection, the church of San Segundo presents the defectology most commonly detected with this technique. Fig. 21 shows the results of the detection of moisture in the main wall. This defect appears as an area at higher temperature, highlighted in black, with continuous thermal evolution towards the healthy area. In this case, temperature is higher in the moisture area because the inspection is performed in the morning when the temperature is higher outside than inside the church. The position and shape of the moisture area leads to the interpretation that moisture is accumulated due to the infiltration of water from the roof.

Another example of detection of moisture is shown in Fig. 22, in this case detected in the wall of the altar. The defect appears at a lower temperature than the healthy area, with a higher intensity towards the ground and decreasing with height. This is due to the

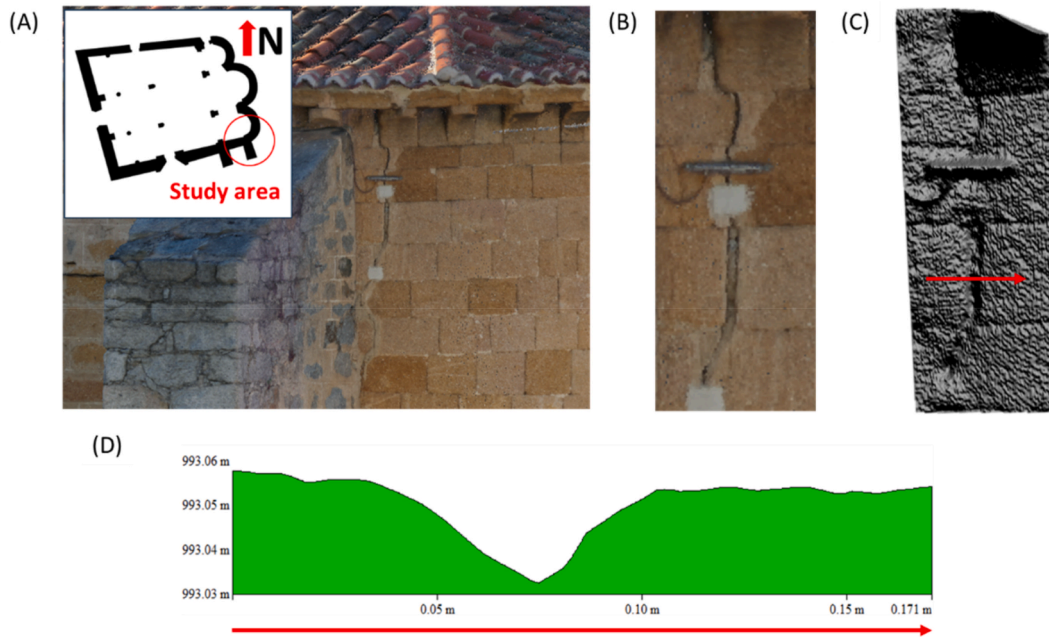


Fig. 14. Crack located in the south apse. (A) 3D point cloud image where the crack can be seen. (B) Detail image of the crack in the 3D point cloud. (C) Elevation grid model of the crack and its surroundings, along with the location where the section was made. (D) Cross section of the crack.

origins of the moisture that can be associated with capillarity. The different temperatures in the surroundings of the moisture area show that although the accumulation of water is not constant, it has had an effect on the material, provoking detachment and delamination at the surface.

A different sign of moisture is detected on the wooden floor of the interior balcony (Fig. 23). In this case, the defect area appears at a lower temperature than the healthy area, probably due to the heating of the wood by the solar radiation coming from the opposite windows. Since water has a lower thermal conductivity than wood, the moisture area needs more time to heat and therefore appears colder in the morning. In this case, the origin of the water is not clear, since the thermal print is not related to any wall communicating with the exterior.

Additionally, Fig. 24 shows the occurrence of air infiltration between the walls of the main façade and the entrance to the church. This air infiltration in an area with a change in geometry is a signal of the occurrence of a thermal bridge, that is, an area where the construction is not completely sealed. As in the moisture defect, the defect appears at a higher temperature than the healthy area because of the inspection being performed in the morning, when outdoor ambient temperature is higher than indoor ambient temperature.

As a complement of the GPR and TLS surveys, thermal infrared images were acquired from the wood beam that supports the balcony, in order to discard the existence of pathologies with thermal affection. Fig. 25 shows the temperature distribution in the wooden beam on the front and horizontal surfaces, that present no clear sign of defects.

Last, the thermographic inspection included the outer surface of the walls, focusing mainly on the back façade, due to several reasons: (1) this façade is the closest to the river, and could be subjected to more severe damages caused by moisture, which has a great effect in the hermitage according to the other defectology detected by the technique; (2) this façade is West – oriented, in such a way that the Sun radiation could not provoke any disturbance in the temperature measurements.

Due to the size of the façade, several thermal infrared images were required in order to cover the complete surface. In order to perform a complete interpretation of the defects possibly affecting the back façade, the images were processed for the generation of a thermal mosaic, as shown in Fig. 26. Thanks to the combination of images in a mosaic, it is possible to have a general view of the façade, in such a way that pathologies that could go unnoticed in their partial appearance in several images can be correctly identified due to their complete representation in the mosaic.

According to the mosaic, no pathologies are detected, but changes in the materials. The different stone types appear at different temperatures, probably due to their different emissivity values. However, at the top of the bells tower there is a change in temperature with no apparent change in stone material, that could be caused by a pathology in the state of the stone or of the adhesive material.

5. Integrated interpretation

The application of the three non-destructive techniques for the integral evaluation of the San Segundo Hermitage shows the importance of the combination of different techniques for the adequate detection and correct identification of the defects.

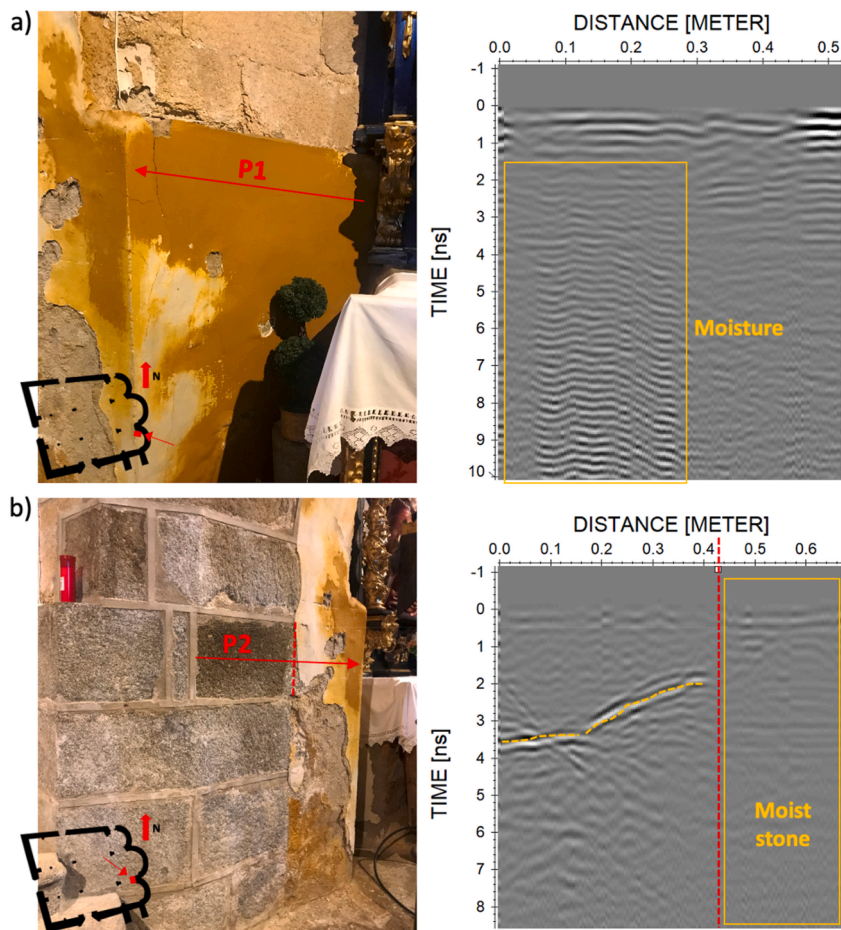


Fig. 15. 2.3 GHz data produced in the side wall of the altar: a) lateral wall, and b) front wall. Moist areas are highlighted into orange boxes, and the red dashed line in b) indicates the separation between apparently healthy stone and disintegrated stone. (For interpretation of the references to colour in this figure legend, the reader is referred to the Web version of this article.)

Table 10 compiles the different applications of the non-destructive tests herein used for the evaluation of the building. First, the capabilities of each technique (in general for any case study) are shown, highlighting then benefits of the combination for the interpretation of our case study. The combination proved to be useful for confirming the existence of defects detected, as well as to complete the interpretation in order to provide the probable cause of damage. For example, in the case of moisture in walls, the three techniques separately detected the presence of moisture in the altar wall, but the TLS and IRT revealed the origin (moisture comes from capillarity) while the GPR provided the extent and depth of the damage in the interior of the structure. Furthermore, the moisture detected in this wall (and disintegrated stone) may be the cause of the structural deformation observed by the TLS at the right nave of the hermitage. However, the origin of this deficiency may be completely different (e.g. an error in the design or construction phase, or settlement phenomena). The integrated interpretation therefore provides more comprehensive knowledge about the condition state and causes of damage affecting the integrity and strengthening of the structure, thus contributing to define more appropriate and effective decision-making solutions for maintenance.

6. Conclusions and future research

The combination of the three non-destructive techniques considered in the present research has allowed a complete and precise evaluation of the Hermitage of San Segundo, identifying defects, determining their causes, and providing a solid basis for future decision-making regarding maintenance and restoration. This comprehensive approach improves the understanding about the state of conservation of the asset, and contributes to the definition of more effective and appropriate solutions to face possible issues affecting the integrity of the building.

In this context, the use of the mentioned procedures has enabled not only to confirm the presence of moisture in the walls (masonry), but also to understand its origin and the magnitude of the damage. Furthermore, the relationship between the walls moisture and the structural deformation observed in the right nave of the hermitage may indicate a possible connection between both pathologies, which is crucial to define effective maintenance solutions. On the other hand, the combination of GPR and IRT was essential to identify moisture in the wooden floor.

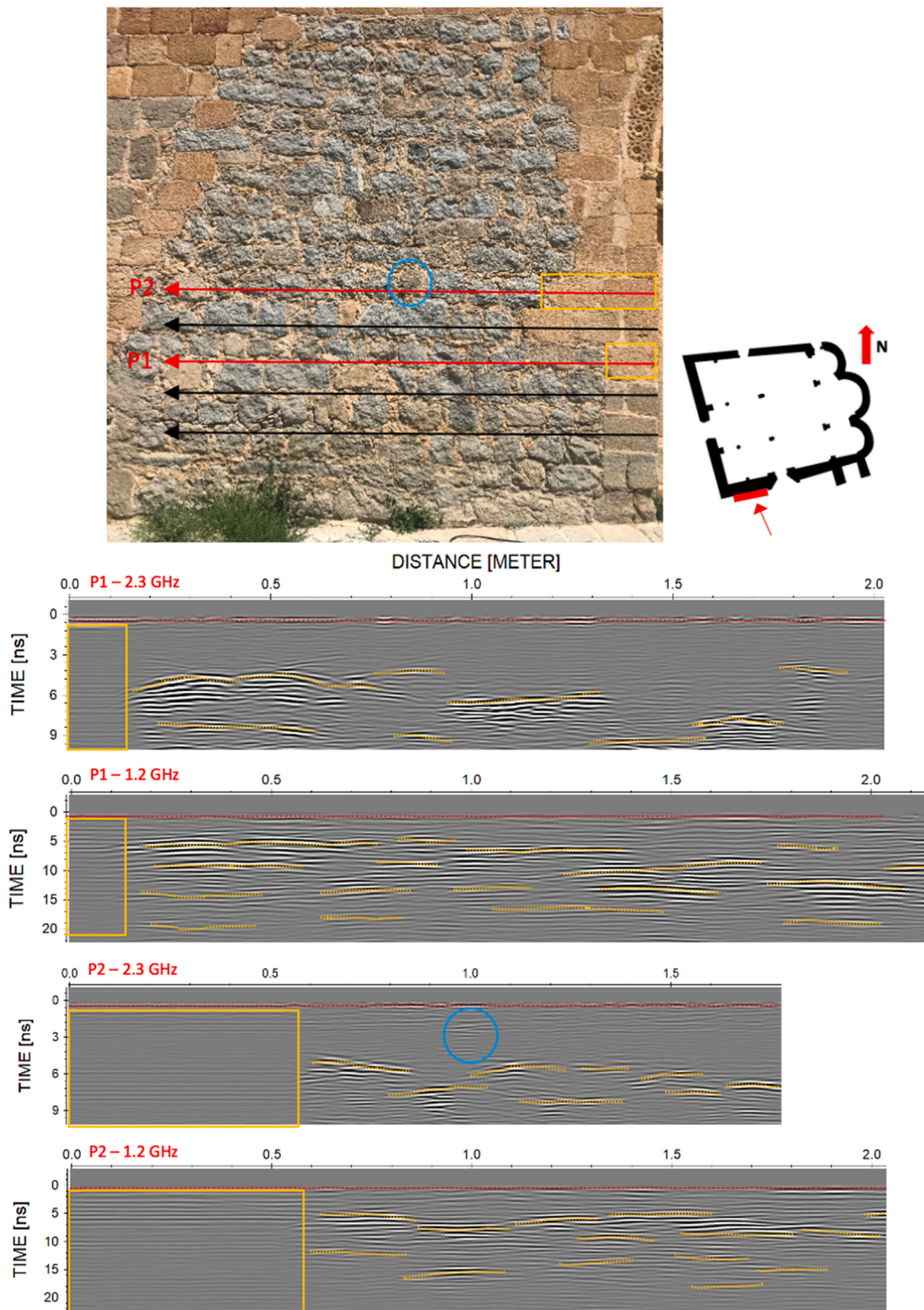


Fig. 16. 2.3 GHz and 1.2 GHz data produced for the characterization of the stonework materials in the external wall of the main façade. Moist areas are highlighted into orange boxes, while different ashlars (thicknesses) are marked with orange dashed line (the red line indicates the surface level), and rough stones are highlighted into a blue ellipse. (For interpretation of the references to colour in this figure legend, the reader is referred to the Web version of this article.)

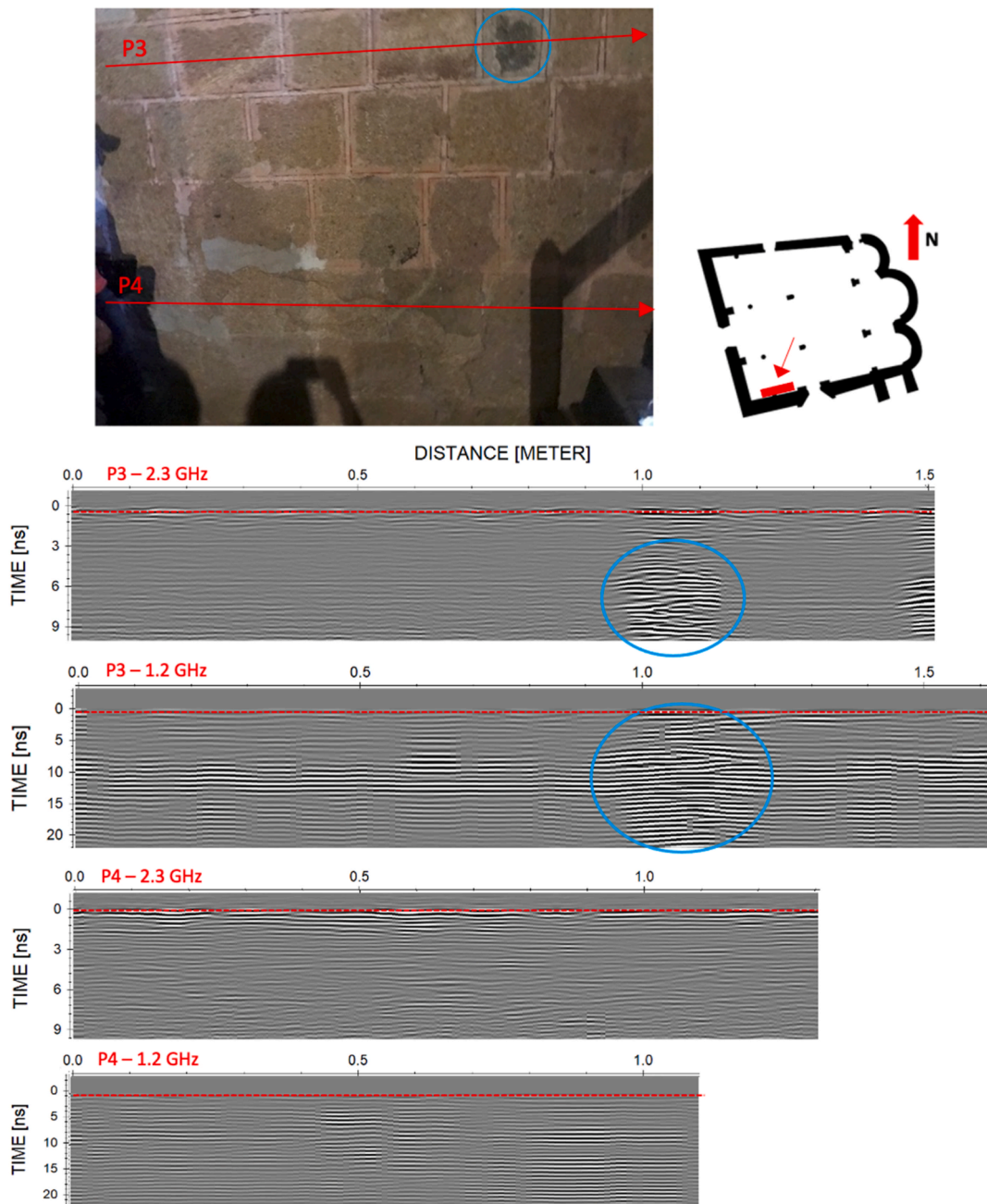


Fig. 17. 2.3 GHz and 1.2 GHz data produced for the characterization of the stonework materials in the internal wall of the main façade. The red line indicates the surface level, and the blue ellipses highlighted rough stones. (For interpretation of the references to colour in this figure legend, the reader is referred to the Web version of this article.)

In the case of stone cracks, results tend to indicate the effectiveness of integrating TLS and GPR techniques. However, IRT did not provide relevant information in this aspect, highlighting the importance of selecting appropriate techniques depending on the pathology that aims to be evaluated. On the contrary, the combination of GPR and IRT was essential to identify cracks in wood, which also underscores the need to use multiple methodologies when addressing different types of damage.

The three techniques were useful for the evaluation of the differences in composition and state of the stone, which can be an important question in order to adequately understand the variability of the construction materials used in the case study and the different construction epochs.

It is also worth highlighting the essential role of GPR for the detection of cavities, and the effectiveness of TLS for locating structural deformations, showing once again the added value of the combination of techniques in order to achieve a complete characterization of the specific building.

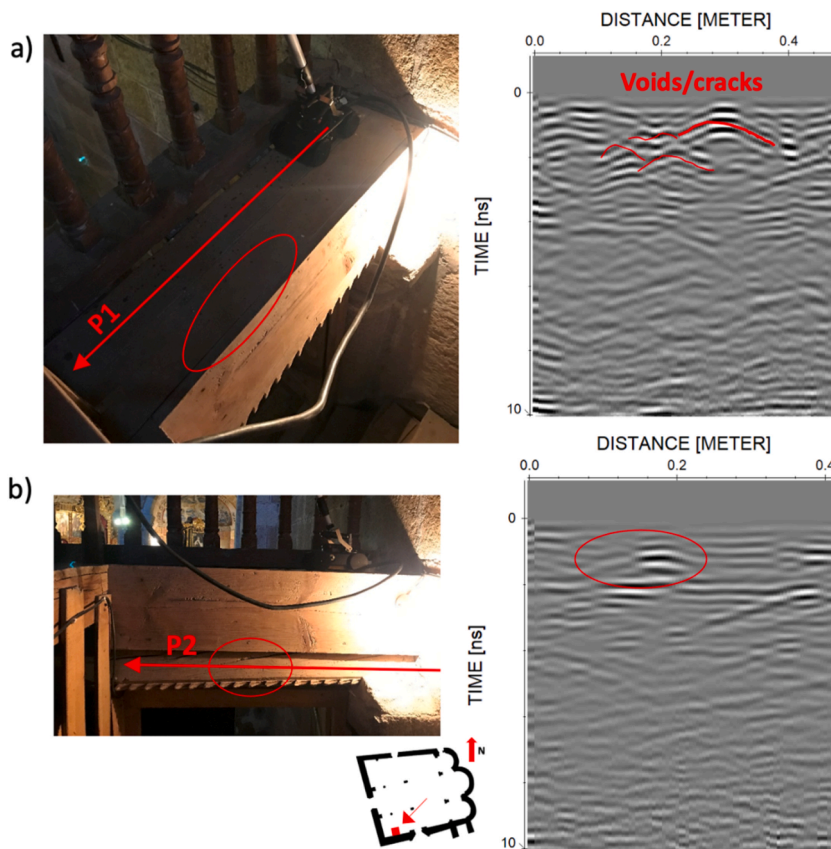


Fig. 18. 2.3 GHz data produced in wooden beams showing the interpretation of voids and cracks (red lines/ellipses): a) superior face and b) lateral face of the beam. (For interpretation of the references to colour in this figure legend, the reader is referred to the Web version of this article.)

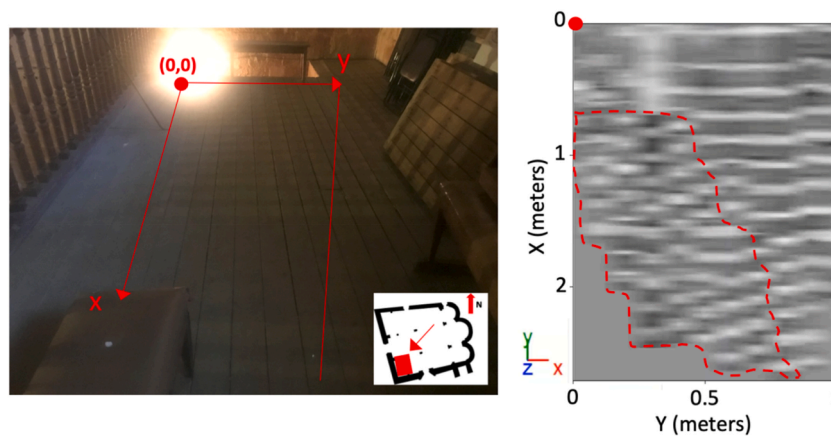


Fig. 19. 1.2 GHz 3D time-slice or XY image at 0.3 ns depth (2.0–2.5 cm considering a velocity of propagation of 13.5–17.4 cm/ns), showing the interpretation of a region with a different signal behavior (highlighted into a dashed red line). (For interpretation of the references to colour in this figure legend, the reader is referred to the Web version of this article.)

In addition, as mentioned before, the point clouds obtained through TLS or photogrammetry allow the implementation of other models such as HBIM or DT that enable the integration of the data derived from the rest of methodologies here considered [68–70]. In this way, a collaborative work environment is achieved where it is possible the geolocation of each of the pathologies identified on the architectural asset, having also a global vision of the conservation state of the building.

Future research will focus on analyzing methodological improvements or alternatives, as well as the possible integration of other prospective methodologies that can contribute to a greater extent to the identification of alternative pathologies and other key aspects for the conservation of existing cultural heritage. Regarding the GPR method, a GPR tomography approach can be performed to ob-

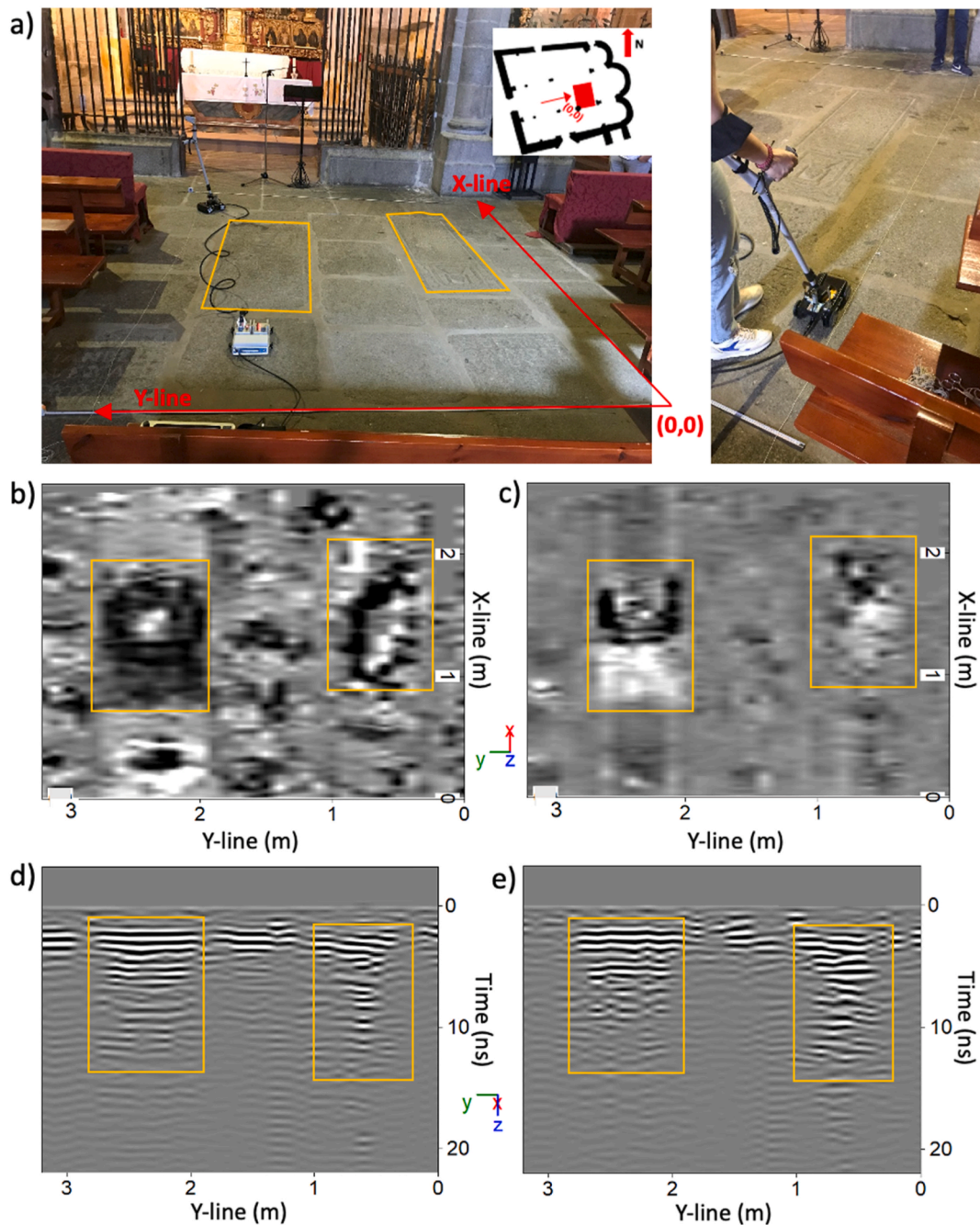


Fig. 20. 1.2 GHz 3D cube highlighting the presence of two hidden tombs (into orange boxes): a) GPR grid, b) time-slice or XY image at 3.6 ns depth (20 cm considering a velocity of propagation of 0.1 m/ns), c) time-slice or XY image at 6 ns depth (30 cm considering a velocity of propagation of 0.1 m/ns), d) YZ image in x-line at 1.4 m, and e) YZ image in x-line at 1.55 m. (For interpretation of the references to colour in this figure legend, the reader is referred to the Web version of this article.)

tain moisture distribution (tomography map), which can be then compared with the thermographic and LiDAR intensity images obtained on the side wall of the altar. Another geophysical method that may complement the GPR information is seismic tomography to detect inner cracks and damages. In addition, DInSAR (Differential Interferometry Synthetic Aperture Radar) technology can be used together with other geophysical and optical techniques as the ones here applied to track movements in the terrain or detect deformations. This strategic combination allows for a more complete and detailed view of the conditions of the heritage environment, providing accurate data on changes in topography that are crucial for effective conservation. On the other hand, IoT (Internet of Things) sensors can be installed in heritage structures or environments to monitor their condition and evolution, as well as detect possible anomalies or risks that may affect their conservation. These devices can measure and transmit data on different physical or chemical para-

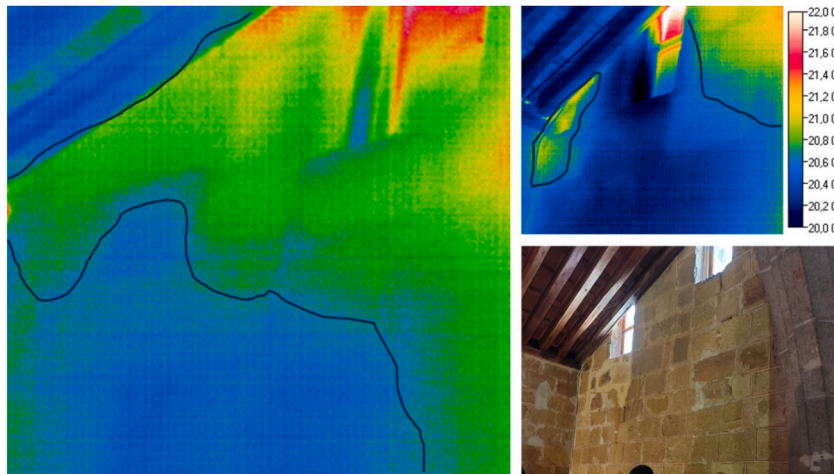


Fig. 21. Moisture detected in the internal surface of the main façade, due to the infiltration of water from the roof.

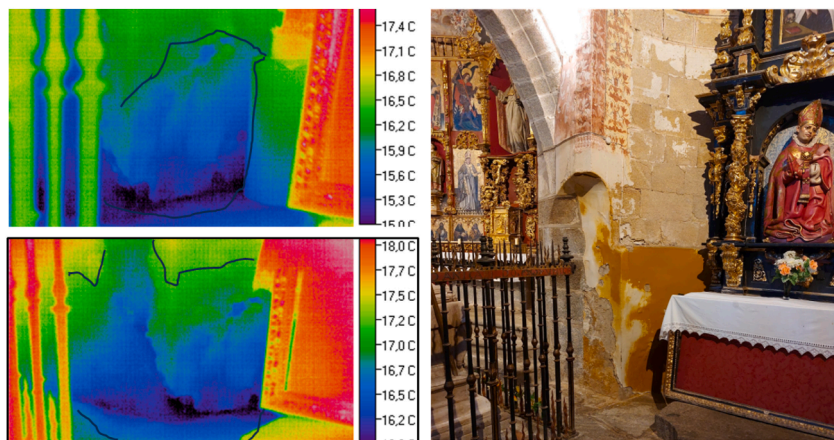


Fig. 22. Delamination in the column of the altar. Damage visible for the human eye; the thermographic inspection allowed to determine that the cause is the entrance of humidity in the walls through capillarity (the temperature increases from the floor upwards).

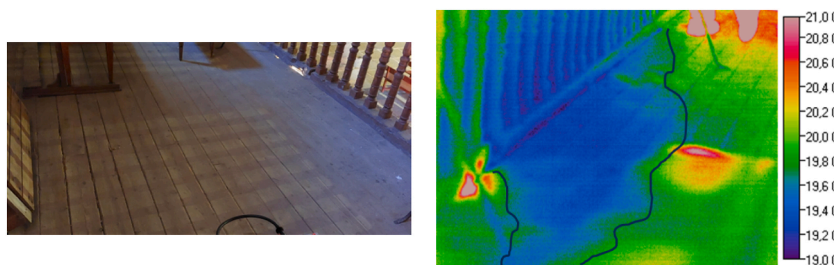


Fig. 23. Moisture detected on the wooden floor of the balcony. The areas that appear at temperatures higher than 21 °C are discarded as pathologies since they are caused by the steps of the operator.

meters, such as temperature, humidity, pressure, vibration, sound, light, gas, etc. As an example, strain gauges can measure deformations or stresses suffered by materials, accelerometers can detect movement or collapse of walls, and other sensors can measure humidity and temperature that influence the degradation of the cultural asset. IoT technology allows these sensors to be connected through low-consumption wireless networks, such as LoRaWAN or Sigfox, which facilitate the transmission of data over long distances and with minimal interference. This data can be stored and processed on cloud platforms, where data analysis, artificial intelligence or machine learning techniques can be applied to extract relevant information and generate alerts or recommendations for the conservation of cultural heritage. In addition, this data can be viewed and shared through web or mobile applications, which allow access and consultation by interested users, such as managers, conservators, restorers, researchers or the general public. The use of

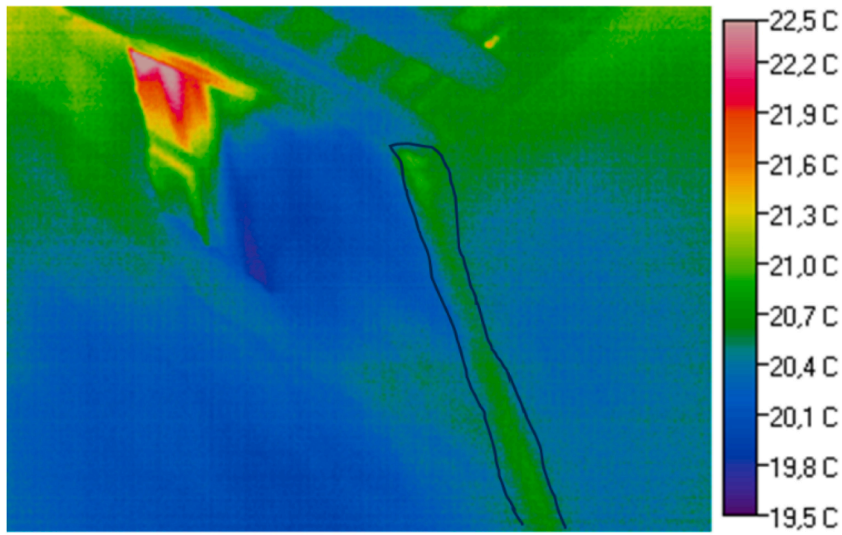


Fig. 24. Air infiltration between walls, signal of a thermal bridge.

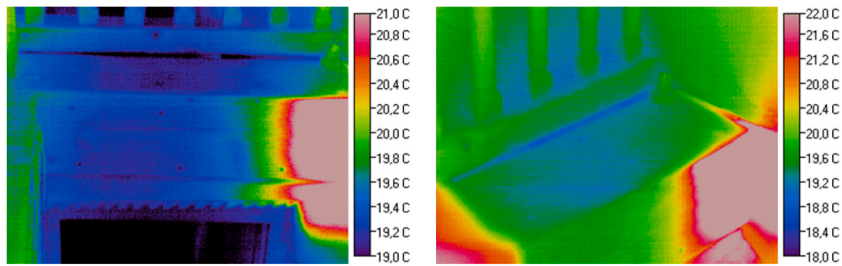


Fig. 25. The wooden beam supporting the balcony does not show any sign of defect with thermal affection.

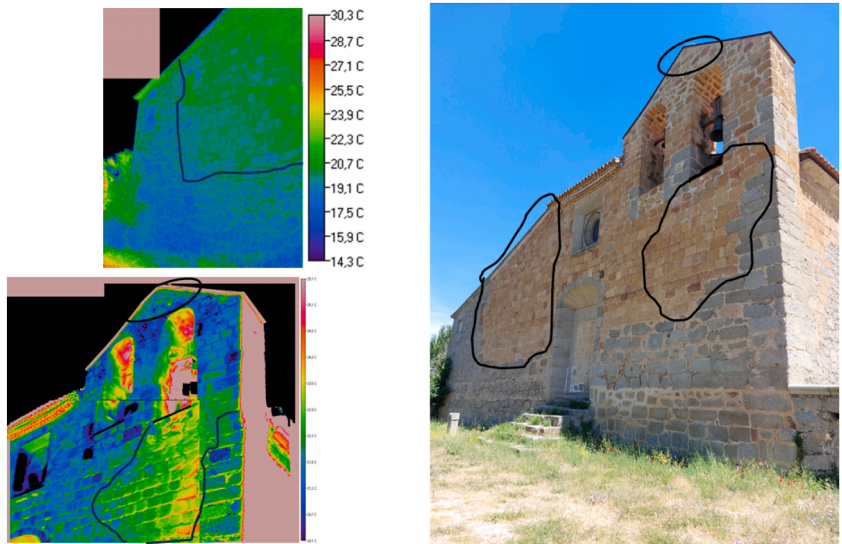


Fig. 26. Thermographic mosaics of the back façade. The black areas indicate the pathologies detected. Top left image represents the area highlighted in black at the left of the façade in the right photograph. Bottom left image represents the area of the bell tower.

Table 10

List of pathologies that can be assessed (in a general way) with each technique separately, and the particular interpretation in the Hermitage of San Segundo, enhancing the benefits of the integrated interpretations.

Pathology	Application in general/Application in the case study			Interpretation in the case study
	TLS	GPR	IRT	
Moisture in walls (masonry)	Yes/Yes	Yes/Yes	Yes/Yes	Moisture from capillarity detected by TLS and IRT; GPR detects the extent and depth of the condition
Moisture in wooden floor	Yes/No	Yes/Yes	Yes/Yes	IRT and GPR detect moisture and their mapping (the TLS method was not herein applied for this purpose)
Cracking in stone	Yes/Yes	Yes/No (under specific conditions of size/depth of the cracks and antenna resolution)	Yes/No (under specific conditions of temperature difference and size/depth of the cracks)	TLS allows to map the extent of surface cracking, while their size makes them not detectable for IRT (the GPR method was not herein applied for this purpose)
Cracking in wooden (floor and beams)	Yes/No (under specific conditions of size/depth of the cracks)	Yes/Yes	Yes/Yes (under specific conditions of temperature difference and size/depth of the cracks)	IRT not detecting the cracks shows that they are small or have low depth; GPR detects some cracks in wooden beams (the TLS method was not herein applied for this purpose).
Different types of stone composition, or condition	Yes/Yes	Yes/Yes	Yes/Yes	TLS and IRT at surface level; GPR detects different materials (or condition) and thicknesses
Cavity detection	No/No	Yes/Yes	Yes/No (under specific conditions of temperature difference and size/depth)	GPR detects buried tombs (the IRT method was not herein applied for this purpose).
Structural deformations	Yes/Yes	No/No	No/No	The TLS allows mapping different structural deformations in heritage assets.

IoT sensors together with the analyzes proposed in the conservation of cultural heritage, offers very promising advantages at a low cost for monitoring the evolution of the heritage asset.

As derived from the above, there are endless possibilities to continue searching for non-destructive solutions for the conservation of cultural heritage where works such as the one presented here significantly contribute to obtaining new information about the pathologies and damages affecting architectural assets.

Founding sources

This work has received funding from the Xunta de Galicia through the project ENDITÍ (Ref. ED431F 2021/08). Mercedes Solla acknowledges the grant RYC2019–026604–I funded by MCIN/AEI/10.13039/501100011033 and by “ESF Investing in your future”. Miguel Ángel Maté-González and Cristina Sáez Blázquez acknowledge the grants RYC2021-034813-I and RYC2021-034720-I, respectively, funded by the Ministerio de Ciencia e Innovación and by the European Union ‘NextGenerationEU’/PRTR.

CRedit authorship contribution statement

Mercedes Solla: Formal analysis, Investigation, Resources, Supervision. **Miguel Ángel Maté-González:** Formal analysis, Investigation, Resources, Supervision. **Cristina Sáez Blázquez:** Methodology, Supervision, Writing – original draft, Writing – review & editing. **Susana Lagüela-López:** Data curation, Investigation, Resources, Supervision. **Ignacio Martín Nieto:** Methodology, Supervision, Validation.

Declaration of competing interest

The authors declare that they have no known competing financial interests or personal relationships that could have appeared to influence the work reported in this paper.

Data availability

Data will be made available on request.

Acknowledgments

This work has been possible thanks to the collaboration of the “Cofradía de San Segundo” and Juan Pedro Pedrero Gómez that have facilitated access to the heritage asset and have provided highly relevant historical information about it.

Appendix A. Supplementary data

Supplementary data to this article can be found online at <https://doi.org/10.1016/j.job.2024.109295>.

References

- [1] E. Bowitz, K. Ibenholt, Economic impacts of cultural heritage—Research and perspectives, *J. Cult. Herit.* 10 (1) (2009) 1–8.
- [2] J. Li, S. Krishnamurthy, A.P. Roders, P. Van Wesemael, Community participation in cultural heritage management: a systematic literature review comparing Chinese and international practices, *Cities* 96 (2020) 102476.
- [3] H. Hirszenberger, J. Ranogajec, S. Vucetic, B. Lalic, D. Gracanin, Collaborative projects in cultural heritage conservation—management challenges and risks, *J. Cult. Herit.* 37 (2019) 215–224.
- [4] R. Harrison, C. DeSilvey, C. Holtorf, S. Macdonald, N. Bartolini, E. Breithoff, S. Penrose, *Heritage Futures: Comparative Approaches to Natural and Cultural Heritage Practices*, UCL press, 2020.
- [5] G.F. Pehlivan, Condition and characterization analysis of a twentieth century cultural heritage through non-destructive testing (NDT) methods: the case of the Sivas industry school ironworking atelier in Turkey, *Heritage Science* 11 (1) (2023) 1–19.
- [6] J. Huang, Y. Zheng, H. Li, Study of internal moisture condensation for the conservation of stone cultural heritage, *J. Cult. Herit.* 56 (2022) 1–9.
- [7] J.R. Bkrentowski, P. Knyziak, J.A. Pawlowicz, G. Gavardashvili, Historical masonry buildings' condition assessment by non-destructive and destructive testing, *Eng. Fail. Anal.* 146 (2023) 107122.
- [8] M. Korkanç, Deterioration of different stones used in historical buildings within Nigde province, Cappadocia, *Construct. Build. Mater.* 48 (2013) 789–803.
- [9] J. Earl, A. Saint, *Building Conservation Philosophy*, Routledge – Taylor & Francis Group, 2015.
- [10] A.M. Korzhenkov, A. Minchev, V. Tenekedjiev, A.N. Ovsyuchenko, O. Dimitrov, A.S. Larkov, A.A. Strelnikov, Seismic deformations in an early Christian monastery in the area of Djanavara, Varna, Bulgaria. Part 1: study methods, *Seism. Instrum.* 57 (3) (2021) 343–359.
- [11] Ž. Savković, M. Stupar, N. Unković, A. Knežević, J. Vukojević, M. Ljaljević Grbić, Fungal deterioration of cultural heritage objects, *Biodegradation Technology of Organic and Inorganic Pollutants* (2021) 267–288.
- [12] J.K. Oh, J.J. Lee, Feasibility of ultrasonic spectral analysis for detecting insect damage in wooden cultural heritage, *J. Wood Sci.* 60 (2014) 21–29.
- [13] A.L. Monaco, F. Balletti, C. Pelosi, Wood in cultural heritage. Properties and conservation of historical wooden artefacts, *Eur. J. Sci. Theol* 14 (2018) 161–171.
- [14] V. Perez-Gracia, M. Solla, S. Fontul, Analysis of the GPR signal for moisture detection: application to heritage buildings, *Int. J. Architect. Herit.* (2022) 1–24.
- [15] I. Garrido, M. Solla, S. Lagüela, M. Rasol, Review of InfraRed thermography and ground-penetrating radar applications for building assessment, *Adv. Civ. Eng.* 2022 (2022).
- [16] D.M. McCann, M.C. Forde, Review of NDT methods in the assessment of concrete and masonry structures, *NDT E Int.* 34 (2) (2001) 71–84.
- [17] F. Lombardi, F. Podd, M. Solla, From its core to the niche: insights from GPR applications, *Rem. Sens.* 14 (13) (2022) 3033.
- [18] M. Rucka, E. Wojtczak, M. Zielińska, Interpolation methods in GPR tomographic imaging of linear and volume anomalies for cultural heritage diagnostics, *Measurement* 154 (2020) 107494.
- [19] Ł. Drobiec, R. Jasiński, W. Mazur, Accuracy of eddy-current and radar methods used in reinforcement detection, *Materials* 12 (7) (2019) 1168.
- [20] A. Novo, H. Lorenzo, F.I. Rial, M. Solla, Three-dimensional Ground-penetrating radar strategies over an indoor archaeological site: convent of Santo Domingo (Lugo, Spain), *Archaeol. Prospect.* 17 (2010) 213–222.
- [21] L. Binda, A. Saisi, C. Tiraboschi, S. Valle, C. Colla, M. Forde, Application of sonic and radar tests on the piers and walls of the Cathedral of Noto, *Construct. Build. Mater.* 17 (8) (2003) 613–627.
- [22] E. Zendri, L. Falchi, F.C. Izzo, Z.M. Morabito, G. Driussi, A review of common NDTs in the monitoring and preservation of historical architectural surfaces, *Int. J. Architect. Herit.* 11 (7) (2017) 987–1004.
- [23] T. Shiotani, S. Momoki, H. Chai, D.G. Aggelis, Elastic wave validation of large concrete structures repaired by means of cement grouting, *Construct. Build. Mater.* 23 (7) (2009) 2647–2652.
- [24] V.G. Haach, F.C. Ramirez, Qualitative assessment of concrete by ultrasound tomography, *Construct. Build. Mater.* 119 (2016) 61–70.
- [25] W. Neubauer, C. Gugl, M. Scholz, G. Verhoeven, I. Trinks, K. Löcker, M. Doneus, T. Saey, et al., The discovery of the school of gladiators at Carnuntum Austria, *Antiquity* 88 (339) (2014) 173–190.
- [26] D.C. Nobes, L.R. Wallace, Geophysical imaging of an early nineteenth century colonial defensive blockhouse: applications of EM directionality and multi-parameter imaging, in: *Archaeogeophysics: Natural Science in Archaeology*, Springer, New York, 2019, pp. 219–232.
- [27] V. Pérez-Gracia, J.O. Cásenles, J. Clapés, G. Martínez, R. Osorio, Non-destructive analysis in cultural heritage buildings: evaluating the Mallorca cathedral supporting structures, *NDT&E International* 59 (2013) 40–47.
- [28] S. Del Pozo, J. Herrero-Pascual, B. Felipe-García, D. Hernández-López, P. Rodríguez-González, D. González-Aguilera, Multispectral radiometric analysis of façades to detect pathologies from active and passive remote sensing, *Rem. Sens.* 8 (1) (2016) 80.
- [29] S. Del Pozo, J. Herrero-Pascual, B. Felipe-García, D. Hernández-López, P. Rodríguez-González, D. González-Aguilera, Multi-sensor radiometric study to detect pathologies in historical buildings, *Int. Arch. Photogram. Rem. Sens. Spatial Inf. Sci.* 40 (2015) 193–200.
- [30] I. Garrido, S. Lagüela, P. Arias, Infrared thermography's application to infrastructure inspections, *Infrastructures* 3 (3) (2018) 35.
- [31] I. Puente, M. Solla, S. Lagüela, J. Sanjurjo-Pinto, Reconstructing the Roman site "Aquis Querquennis" (Bande, Spain) from GPR, T-lidar and IRT data fusion, *Rem. Sens.* 10 (3) (2018) 379.
- [32] B. Lunden, Aerial thermography: a remote sensing technique applied to detection of buried archaeological remains at a site in Dalecarlia, Sweden, *Geogr. Ann. Ser. A Phys. Geogr.* 67 (1985) 161–166.
- [33] P. Vázquez, C. Tomachot-Schneider, Infrared thermography as a tool to detect increasing cracking in granitic stones exposed to high temperatures, *J. Cult. Herit.* 59 (2023) 163–170.
- [34] I. Garrido, E. Barreira, R. Almeida, S. Lagüela, Introduction of active thermography and automatic defect segmentation in the thermographic inspection of specimens of ceramic tiling for building façades, *Infrared Phys. Technol.* 121 (2022) 104012.
- [35] I. Garrido, S. Lagüela, S. Sfarra, H. Zhang, X. Maldague, Automatic detection and delimitation of internal moisture in mosaics from thermographic sequences. Experimental tests, 15th International Workshop on Advanced Infrared Thermography and Applications 27 (1) (2019) 7.
- [36] M. Solla, S. Lagüela, N. Fernández, I. Garrido, Assessing rebar corrosion through the combination of nondestructive GPR and IRT methodologies, *Rem. Sens.* 11 (14) (2019) 1705.
- [37] J.L. Bodnar, J.L. Nicolas, K. Mouhoubi, V. Detalle, Stimulated infrared thermography applied to thermophysical characterization of cultural heritage mural paintings, *Eur. Phys. J. Appl. Phys.* 60 (2) (2012) 21003.
- [38] M. Solla, S. Lagüela, B. Riveiro, H. Lorenzo, Non-destructive testing for the analysis of moisture in the masonry arch bridge of Lubians (Spain), *Struct. Control Health Monit.* 20 (11) (2013) 1366–1376.
- [39] M. Kroustallaki, K. Lampropoulos, E. Delegou, E. Alexakis, A. Tsagarakis, H. Mouzakis, M. Korres, A. Moropoulou, Diagnostic research of the dome of the superstructure of the holy aedicule of the holy sepulchre in Jerusalem – suggestions for maintenance and rehabilitation, in: A. Osman, A. Moropoulou (Eds.), *Nondestructive Evaluation and Monitoring Technologies, Documentation, Diagnosis and Preservation of Cultural Heritage*. Springer Proceedings in Materials, Springer, Cham, 2019, https://doi.org/10.1007/978-3-030-25763-7_1.
- [40] C. Boardman, P. Bryan, *3D Laser Scanning for Heritage: Advice and Guidance on the Use of Laser Scanning in Archaeology and Architecture*, Historic England, 2018.
- [41] Z. Xu, L. Wu, Y. Shen, F. Li, Q. Wang, R. Wang, Tridimensional reconstruction applied to cultural heritage with the use of camera-equipped UAV and terrestrial laser scanner, *Rem. Sens.* 6 (11) (2014) 10413–10434.
- [42] M.G. Gomes, A. Tomé, A digital and non-destructive integrated methodology for heritage modelling and deterioration mapping. The case study of the Moorish Castle in Sintra, *Developments in the Built Environment* 14 (2023) 100145.
- [43] A. Menezes, M.G. Gomes, I. Flores-Colen, In-situ assessment of physical performance and degradation analysis of rendering walls, *Construct. Build. Mater.* 75 (2015) 283–292.
- [44] V. Raimondi, L. Palombi, A. Morelli, M. Chimenti, S. Penoni, U. Dercks, G. Tonini, An integrated multi-medial approach to cultural heritage conservation and documentation: from remotely-sensed lidar imaging to historical archive data, *Earth Resources and Environmental Remote Sensing/GIS Applications VI* 9644

- (2015, October) 45–53 SPIE.
- [45] M. Giroto, F. Rinaudo, F.G. Tonolo, A. Spanò, 3D thermal mapping of architectural heritage, in: *Digital Heritage. Progress in Cultural Heritage: Documentation, Preservation, and Protection: 8th International Conference, EuroMed 2020, Virtual Event, November 2–5, 2020, Revised Selected Papers*, vol. 12642, Springer Nature, 2021, April, p. 26.
- [46] M. Cozzolino, E. Di Giovanni, P. Mauriello, S. Piro, D. Zamuner, *Geophysical Methods for Cultural Heritage Management*, Springer, Cham, Switzerland, 2018, p. 211.
- [47] I. Garrido, M. Solla, S. Lagüela, M. Rasol, Review of InfraRed thermography and ground-penetrating radar applications for building assessment, *Adv. Civ. Eng. 2022* (2022).
- [48] B. Tejedor, D. Bienvenido-Huertas, *Diagnosis of Heritage Buildings by Non-destructive Techniques*, Elsevier, 2024.
- [49] G. Leucci, G. Leucci, Nondestructive testing technologies for cultural heritage: overview, in: *Nondestructive Testing for Archaeology and Cultural Heritage: A Practical Guide and New Perspectives*, 2019, pp. 15–73.
- [50] D. Goodman, S. Piro, *GPR Remote Sensing in Archaeology*, vol. 9, Springer, New York, 2013, p. 233.
- [51] V. Pérez-Gracia, M. Solla, S. Fontul, Analysis of the GPR signal for moisture detection: application to heritage buildings, *Int. J. Architect. Herit.* 18 (2) (2024) 230–253.
- [52] F. Porcelli, L. Sambuelli, C. Comina, A. Spanò, A. Lingua, A. Calantropio, V. De Ruvo, Integrated geophysics and geomatics surveys in the valley of the kings, *Sensors* 20 (6) (2020) 1552.
- [53] D. Zhang, Z. Wu, D. Shi, J. Li, Y. Lu, Integration of terrestrial laser scanner (TLS) and ground penetrating radar (GPR) to characterize the three-dimensional (3D) geometry of the Maoyaba segment of the Litang fault, Southeastern Tibetan plateau, *Rem. Sens.* 14 (24) (2022) 6394.
- [54] E.T. Delegou, G. Mourgi, E. Tsilimantou, C. Ioannidis, A. Moropoulou, A multidisciplinary approach for historic buildings diagnosis: the case study of the Kaisariani monastery, *Heritage* 2 (2) (2019) 1211–1232.
- [55] I. Garrido, M. Solla, S. Lagüela, N. Fernández, IRT and GPR techniques for moisture detection and characterisation in buildings, *Sensors* 20 (22) (2020) 6421.
- [56] M. Abeledo, Ávila 1517-1519, la fundación de un pasado legendario: La invención de san Segundo. e-Spania, *Revue interdisciplinaire d'études hispaniques médiévales et modernes* (33) (2019).
- [57] M. Fernández-Shaw Toda, *Carpintería de lo blanco en la provincia de Avila (Arquitectura religiosa)*, 1994.
- [58] A. Diéguez Rodríguez, Una pequeña Virgen de la Leche del Maestro de las Medias Figuras en el convento de carmelitas descalzas de San José de Ávila, *BSAA Arte: Boletín del Seminario de Estudios de Arte* (71) (2005) 343–348.
- [59] M. Solla, GPR dataset San Segundo hermitage (Ávila, Spain), *Zenodo* (2024), <https://doi.org/10.5281/zenodo.10670222>.
- [60] M.Á. Maté González, M. Solla, C. Sáez-Blázquez, S. Lagüela, I. Martín-Nieto, Laser scanning intensity image data applied to damage detection, *Zenodo* (2024), <https://doi.org/10.5281/zenodo.10681004>.
- [61] D. Gonzalez-Aguilera, L. López-Fernández, P. Rodriguez-Gonzalvez, D. Hernandez-Lopez, D. Guerrero, F. Remondino, F. Menna, E. Nocerino, I. Toschi, A. Ballabeni, et al., GRAPHOS—open-source software for photogrammetric applications, *Photogramm. Rec.* 33 (2018) 11–29.
- [62] S. Lagüela, Thermal infrared dataset in san Segundo hermitage, *Zenodo* (2024), <https://doi.org/10.5281/zenodo.10696251>.
- [63] J. Armesto-González, B. Riveiro-Rodríguez, D. González-Aguilera, M.T. Rivas-Brea, Terrestrial laser scanning intensity data applied to damage detection for historical buildings, *J. Archaeol. Sci.* 37 (12) (2010) 3037–3047.
- [64] J.T. Tou, R.C. Gonzalez, *Pattern Recognition Principles*, 1974.
- [65] J. Armesto-González, B. Riveiro-Rodríguez, D. González-Aguilera, M.T. Rivas-Brea, Terrestrial laser scanning intensity data applied to damage detection for historical buildings, *J. Archaeol. Sci.* 37 (12) (2010) 3037–3047.
- [66] G. Vacca, Overview of open source software for close range photogrammetry, *Int. Arch. Photogram. Rem. Sens. Spatial Inf. Sci.* 42 (2019) 239–245.
- [67] F. Comisi, L. De Giorgi, G. Leucci, Integrated use of GPR and TDR for wood permittivity evaluation, in: *Proc. IMEKO TC-4 Int. Conf. Metrol. Archaeol. Cultural Heritage*, 2020, pp. 1–4.
- [68] M. Solla, L.M. Gonçalves, G. Gonçalves, C. Francisco, I. Puente, P. Providência, H. Rodrigues, A building information modeling approach to integrate geomatic data for the documentation and preservation of cultural heritage, *Rem. Sens.* 12 (24) (2020) 4028.
- [69] R. Mora, L.J. Sánchez-Aparicio, M.Á. Maté-González, J. García-Álvarez, M. Sanchez-Aparicio, D. González-Aguilera, An historical building information modelling approach for the preventive conservation of historical constructions: application to the Historical Library of Salamanca, *Autom. Construct.* 121 (2021) 103449.
- [70] L.J. Sánchez-Aparicio, R. Mora, B. Conde, M.Á. Maté-González, M. Sánchez-Aparicio, D. González-Aguilera, Integration of a wearable mobile mapping solution and advance numerical simulations for the structural analysis of historical constructions: a case of study in San Pedro Church (Palencia, Spain), *Rem. Sens.* 13 (7) (2021) 1252.